Rapid hypothalamic-pituitary recovery after chronic glucocorticoid therapy enables strategies that prevent adrenal suppression

Lindsey S. Gaston[1], Brenna C. Jorgensen[1], Hannah R. Friedman[1], Marc S. Sherman[2], Joseph A. Majzoub[1]

Affiliations:

[1]Division of Endocrinology, Department of Pediatrics, Boston Children's Hospital, Harvard Medical School, Boston, MA, USA

[2]Division of Gastroenterology, Department of Medicine, Massachusetts General hospital, Harvard Medical School, Boston, MA, USA

Conflict-of-interest Statement: The authors have declared that no conflict of interest exists

ABSTRACT

Glucocorticoid-induced adrenal insufficiency (GIAI) persists for months to years after long-term treatment, which past studies suggest is mediated by initial, post-withdrawal hypothalamic-pituitary suppression. We examined the timing of hypothalamic, pituitary, and adrenal (HPA) recovery after 8 weeks of dexamethasone (DEX) treatment in mice. At withdrawal, HPA function was fully suppressed, but *Crh* mRNA and plasma ACTH surprisingly rebounded above control levels within 1 week. Despite this, corticosterone (CORT) remained suppressed for an additional 7 weeks. DEX-exposed adrenals were atrophic and contained previously undescribed, giant, multinucleated histiocytes. CORT secretion was disproportionately low relative to the non-histocyte adrenocortical area in the first 1-2 weeks post-DEX, suggesting that post-withdrawal GIAI is mediated by adrenocortical atrophy with superimposed, reduced ACTH responsiveness. We then tested whether trophic stimulation of the adrenal during glucocorticoid exposure prevented GIAI. Daily co-treatment with DEX and cosyntropin (an ACTH analog) failed to prevent GIAI. However, mice with non-suppressible endogenous ACTH due to knockout of the hypothalamic glucocorticoid receptor maintained normal adrenal function and histology despite long-term DEX. Localizing the mechanisms of post-withdrawal GIAI to the adrenal may permit the development of preventative strategies that mimic native HPA signaling during glucocorticoid exposure, thus reducing the morbidity of a widely prescribed drug class.

INTRODUCTION

Up to 3% of the United States population is prescribed systemic glucocorticoids, and additional patients are chronically treated with topical and inhaled formulations that can exert systemic toxicity even at moderate doses[1-6]. Exogenous glucocorticoids, like native cortisol in humans and corticosterone in rodents, exert glucocorticoid-receptor (GR)-mediated feedback inhibition on the central nodes of the HPA axis, leading to decreased synthesis and secretion of hypothalamic corticotropin-releasing hormone (CRH) and pituitary adrenocorticopic hormone (ACTH)[7]. ACTH not only acutely drives steroidogenesis but is also a key trophic factor for the adrenal gland[8,9]. In fact, Wyllie and Kerr's earliest morphologic descriptions of apoptosis were in ACTH-deprived adrenals, via either hypophysectomy or short-term prednisolone treatment, which was rescued by concurrent, intraperitoneal ACTH injections[8,10].

Hypothalamic-pituitary-adrenal (HPA) axis suppression is typically transient in patients treated with short-term glucocorticoids; however, treatment exceeding four weeks can cause protracted adrenal insufficiency that can persist for weeks up to years after steroid withdrawal[11-13]. While the axis awaits recovery, individuals are at risk for adrenal crisis with otherwise routine illnesses or trauma, which has been associated with longer hospitalizations, higher rates of ICU admissions, and even death in patients who are not promptly administered stress-dose steroids[14,15]. Despite the ubiquity of glucocorticoid use and the healthcare burden of glucocorticoid-induced iatrogenic adrenal insufficiency (GIAI), the mechanisms of persistent HPA axis dysfunction after discontinuation of steroid treatment remain unknown[14]. Elucidation of these processes may lead to novel therapies that either prevent or hasten recovery from GIAI.

Humans are thought to recover from GIAI by reversal of sequential phases of post-withdrawal central and adrenocortical dysfunction. This is based on the work of Graber and colleagues, who found that patients exposed for a year or more to glucocorticoids had inappropriately low to normal ACTH levels for the first 1-2 months after steroid withdrawal despite release from negative feedback. Basal cortisol required another 5-9 months to normalize even after ACTH rebounded

above control levels[16]. Post-withdrawal central suppression has also been described in patients treated for Cushing disease, a state of chronic, endogenous ACTH excess driven by an ACTH-secreting pituitary adenoma[17-20]

Given the evolutionary conservation of the mammalian HPA axis, animal models may address the limitations of clinical studies in defining the anatomic locus and mechanisms of post-withdrawal GIAI[21]. Interestingly, all rodent studies-to date have demonstrated rapid restoration of hypothalamic-pituitary function after steroid treatment. Basal and stimulated ACTH levels (following lipopolysaccharide, arecholine, and CRH administration) were recovered within days of discontinuing 5 or 7 days of methylprednisolone or dexamethasone, respectively, in rats[22,23]. In mice treated with dexamethasone for 30 days, plasma ACTH and corticotroph *Pomc* mRNA levels were elevated above control animals by 1-week post-withdrawal[24]. In all studies, corticosterone (CORT) levels and/or steroidogenic pathway gene expression remained low 5-7 days after discontinuing steroids depiste normalization of adrenal weights[22-24]. No preclinical studies to date have examined HPA axis recovery after longer courses of glucocorticoids known to cause protracted adrenal suppression in humans.

To identify the rate-limiting steps in HPA axis recovery and the mechanisms underlying protracted GIAI following long-term glucocorticoid treatment, we evaluated the temporal dynamics of hypothalamic, pituitary, and adrenal recovery in mice withdrawn from an 8-week dexamethasone (DEX) regimen. After finding that CORT secretion remained supressed for 8 weeks after DEX withdrawal despite rapid restoration of hypothalamic-pituitary function, we attempted to prevent GIAI by providing sustained trophic stimulation to the adrenal during glucocorticoid exposure using either a pharmacologic or genetic approach. Overall, we found that the adrenal is the major anatomic locus of post-withdrawal GIAI and is an accessible therapeutic target for strategies to prevent long-term, post-withdrawal adrenal suppression.

RESULTS

Mice treated with long-term DEX have protracted adrenal insufficiency despite early hypothalamic-pituitary recovery

We first established when hormonal function recovered at each node of the HPA axis following long-term DEX treatment. Adult, male, WT mice were treated with continuous DEX in drinking water for 8 weeks. Starting at the time of DEX withdrawal (8+0) and at 1-2 week intervals through 8+8 (where 8 weeks of treatment plus N weeks of withdrawal = 8+N), ACTH and corticosterone (CORT) were measured in the basal, unstimulated state at 16:30 followed by necroscopy for evaluation of hypothalamic *Crh* mRNA expression by *in situ hybridization* (Model 1, Fig. 1).

As expected, long-term DEX treatment suppressed *Crh* mRNA within the paraventricular nucleus of the hypothalamus (PVH; 28±5 in 8+0 vs. 156±32 arbitrary units [AU] in DEX-naïve (DN) animals, $p<0.05$). Expression recovered to control levels 1 week after DEX was discontinued (8+1; 159±28 AU, $p>0.9999$ vs. DN, Fig. 2A, B). Plasma ACTH levels in the unstimulated, basal state were similarly suppressed on DEX (8+0; 6.1±6.1 pg/mL) but rebounded above controls (DN; 306±125) by 1-week post-withdrawal (1450±207, $p<0.001$, Fig. 2C). This elevation in basal ACTH secretion persisted until 8 weeks post-withdrawal. Basal CORT levels were undetectable on long-term DEX and gradually recovered in the 6 weeks following treatment completion, although differences between DEX-withdrawn and DEX-naïve animals did not reach statistical significance owing to expected variability in unstimulated hormone measurements (Fig. 2D).

In separate, terminal cohorts of mice, we then performed insulin-induced hypoglycemia and cosyntropin-stimulation testing followed by necroscopy at 1-2 week intervals after withdrawal of 8 weeks DEX, as above (Model 1, Fig. 1). Each of these provocative tests has been used to clinically diagnose AI by evaluating HPA axis responsiveness to a physiologically-relevant stressor and maximal CORT secretion to a standardized, pharmacologic stimulus, respectively. As expected, IIH-stimulated ACTH (4.2±3.6 pg/mL) and CORT (1.0±0.24 mcg/dL) as well as cosyntropin-stimulated CORT (2.0±0.61 mcg/dL) levels were suppressed at the completion of

125 DEX treatment (8+0) relative to DN controls (875±44 pg/mL, 27±1.1 mcg/dL, and 15.7±1.2 mcg/dL
126 for IIH-stimulated ACTH, IIH-stimulated CORT, and cosyntropin-stimulated CORT, respectively;
127 $p<0.001$ for all, Fig 1E-G). However, by one week post-withdrawal (8+1), IIH-stimulated ACTH
128 levels (1707±85 pg/mL) were surprisingly elevated above DN control values (875±44 pg/mL,
129 $p<0.001$). IIH-stimulated ACTH levels remained elevated through 4 weeks post-withdrawal and
130 reached a peak two weeks after completion of DEX treatment (Fig. 1E).

131 Despite this supraphysiologic ACTH stimulation, both IIH-stimulated (Fig. 1F) and
132 cosyntropin-stimulated CORT levels (Fig. 1G) remained significantly lower than DN-controls until
133 8 weeks post-DEX withdrawal. Recovery of both IIH-stimulated and cosyntropin-stimulated CORT
134 secretion was modeled with exponential growth equations yielding doubling times of 2.4 (R^2=0.89;
135 replicates test for lack of fit p=0.0001) and 2.5 weeks (R^2=0.86; replicates test for lack of fit
136 p=0.1056), respectively (Fig. S1A-B). Mice withdrawn from long-term DEX thus have delayed
137 recovery of CORT secretion despite rapid restoration of hypothalamic-pituitary function.

138

139 *Long-term DEX induces adrenocortical atrophy with accumulation of giant histiocyte clusters*

140 As the above studies implicate the adrenal rather than the hypothalamus or pituitary as the
141 major anatomic locus of post-withdrawal HPA axis dysfunction, we then assessed adrenal mass
142 and morphology at select time points after long-term DEX treatment. Long-term DEX treatment
143 reduced adrenal weights to 40% of controls (1.0±0.041 mg in 8+0 vs. 2.5±0.063 mg in DN,
144 $p<0.0001$, Fig. 3A). Although adrenals from DEX-exposed adrenals weighed significantly less
145 than those from DN controls through 6 weeks post-withdrawal, distinct patterns of recovery were
146 noted for adrenal mass vs. function. In particular, adrenal mass nearly doubled between 0 to 1
147 weeks post-withdrawal to 75% of controls (1.9±0.11 mg at 8+1) and remained relatively stable
148 over the remaining recovery period. In contrast, CORT secretion remained 75% lower than control
149 values at 8+1 and more gradually recovered over the subsequent 7 weeks (Fig. S1A and B; raw
150 data derived from Fig. 2E and F and 3A).

151 Hematoxylin and eosin staining revealed that long-term DEX caused massive, adrenocortical
152 atrophy followed by gradual reaccumulat ion of cortical tissue in the 8 weeks following
153 glucocorticoid withdrawal. Interestingly, DEX-exposed adrenals contained large, vacuolated
154 structures with reduced nuclear density near the corticomedullary junction that persisted through
155 8 weeks post-withdrawal (Fig. 3B, magnification in 3C). These clusters were intensely
156 autofluorescent, which was markedly attenuated with the addition of TrueBlack, a lipofuscin
157 autofluorescence quencher[25] (Fig. 3D). ISH with a 5'-Cy5-Oligod(T)30 demonstrated similar,
158 nuclear mRNA poly(A) content in these structures compared to surrounding cortical cells[26,27]. The
159 large, vacuolated, extranuclear space in these clusters was not strongly labeled with 568 NHS
160 Ester (SE), a total protein stain[28,29]. Together, this suggests that the multinucleated clusters
161 observed in DEX-exposed adrenals contain live, lipofuscin-containing, biologically active cells
162 rather than acellular, proteinaceous debris.

163 We then asked whether these cells represented an atypical steroidogenic population vs.
164 histiocytes, the latter of which have been identified using morphologic characteristics in rat
165 adrenals following short-term glucocorticoid treatment[10,30]. Immunofluorescence for the myeloid-
166 specific surface marker CD68 was performed on adrenals exposed to 2-8 weeks DEX (2+0, 4+0,
167 and 8+0), as well as those withdrawn from 8-weeks DEX for 1 and 8 weeks (8+1 and 8+8). Glands
168 were counterstained with fluorescent (488)-congugated streptavidin, which labels all
169 steroidogenic cells of the adrenal cortex[31], and TrueBlack to quench lipofuscin autofluorescence
170 (Fig. 4). Rare, mononuclear, CD68-positive cells were visualized in dexamethasone naïve glands.
171 More numerous CD68 positive cells were present throughout the zona fasciculata (zF) after 2
172 weeks of DEX treatment (2+0), which was followed by larger, apparently mutinuclear CD68+
173 accumulations at the corticomedullary junction with ongoing treatment (at 4+0 and 8+0; Fig. 4A
174 and B). Large, corticomedullary, CD68-positive accumulations remained present at 1-week post-
175 withdrawal (8+1), although these clusters appreared to fragment and migrate centripedally by 8
176 weeks off treatment (8+8; Fig. 4A). Subsequent immunofluorescence with the membrane-bound

177 mouse macrophage marker F4/80 and adrenal medulla marker tyrosine hydroxylase (TH)
178 demonstrated expansion of smaller, single-nucleated macrophage-like cells after 2 weeks of DEX.
179 After 8 weeks of treatment, these cells appeared to aggregate into large, multinuclear, F4/80-
180 positive clusters at the corticomedullary junction, which we herein term "Giant Histiocytes of
181 Steroid Treatment" (GHOSTs; Fig. 4C and D).
182

183 *CORT secretion is disproportionately low relative to steroidogenic cell mass in the first 2 weeks*
184 *after DEX withdrawal*

185 Reasoning that GHOSTs might contribute to adrenal mass but not biosynthetic function, we
186 then asked specifically how the steroidogenic cell population contracted and recovered with
187 prolonged DEX treatment and withdrawal. To do this, we performed morphometric analysis on
188 thick, immunostained adrenal sections, which allowed for comparison of the largest, equatorial
189 adrenal section from each gland. Since no antibodies reliably distinguished adrenocortical cell
190 types in thick, floating section IF pilot studies (data not shown), we first performed standard IF
191 on FFPE tissue using Dab2 and Ki-67, markers of the zG and proliferative cells, respectively[32]
192 (Fig S2). There was no significant change in zona glomerulosa (zG) thickness after long-term
193 DEX treatment (Fig. S2B). The zF had a slight increase in nuclear density at the completion of
194 DEX treatment (8+0 vs. DN, Fig. S2C) but was otherwise unchanged in the period after DEX-
195 withdrawal. A more than 5-fold increase in the proliferative cellular marker, Ki-67, appeared in
196 the zF starting at 1-week post-withdrawal and continued throughout the recovery period (Fig.
197 S2D). Taken together, these data demonstrate that adrenals withdrawn from long-term DEX
198 recover primarily by proliferation of the zF rather than cellular hypertrophy or alterations in zG
199 compartment size, making the pan-cortical area a reasonable surrogate for zF cell counts.
200 Moreover, GHOSTs did not contain the mRNA encoding the CORT biosynthetic enzyme
201 Cyp11b1, suggesting that GHOSTs are not capable of steroidogenisis (Fig. S2E).

202 Following the above FFPE studies, we then performed morphometric analyses of whole,
203 equatorial adrenal slices from DN, 8+0, 8+1, 8+2, 8+6, and 8+8 animals to quantify
204 steroidogenic cell type loss and recovery after long-term DEX treatment (Fig. 5). 488-
205 streptavidin[31] (green) and IF for TH (red), both as above, were used to label steroidogenic vs.
206 medullary cells, respectively. Since sections were not treated with TrueBlack, GHOSTs were
207 labeled by endogenous autofluorescence (cyan; Fig. 5A). Pan-cortical area, which includes both
208 streptavidin-positive and autofluorescent regions, decreased significantly with DEX treatment
209 (480±7 mm^2 in 8+0 vs. 1290±156 mm^2 in DN, $p<0.01$) but normalized by 1-week post-
210 withdrawal (1096±65 mm^2 in 8+1, Fig. 5A and B). Autofluorescent GHOST area increased
211 significantly with DEX treatment and remained stably elevated through 8 weeks post-withdrawal,
212 with fragmentation and centripetal migration at later timepoints (Fig. 5A and C). Steroidogenic
213 cell type area was computed by subtracting GHOSTs (cyan autofluorescence) from the pan-
214 cortical (green) area, which markedly decreased with DEX treatment (272±47 mm^2 in 8+0 vs.
215 1286±153 mm^2 in DN, $p<0.001$) but more than tripled in the first week post-withdrawal
216 (887±70mm^2; Fig. 5D). Medullary (TH-positive) area was comparable at all timepoints, indicating
217 that relatively equivalent, equatorial adrenal sections were used for morphometric analyses
218 ($p=0.15$, Fig. 5E).

219 We next assessed the relationship between maximal CORT secretion to cosyntropin
220 stimulation and the size of the steroidogenic cell population in the recovering adrenal. This was
221 first measured as the ratio of stimulated CORT secretion to the steroidogenic area normalized to
222 this same ratio for DN controls (Fig. 5F). This ratio insignificantly decreased at the completion of
223 DEX treatment (from 1.0±0.12 in DN to 0.62±0.11 in 8+0, $p=0.08$) but was surprisingly lowest at
224 1- and 2- weeks post-DEX (0.46±0.036 and 0.42±0.010; $p<0.05$; Fig. 5F). Conversely, this ratio
225 of stimulated CORT secretion to steroidogenic area was significantly higher at 8 weeks post-
226 DEX (1.8±0.11, $p<0.01$) vs. DN.

227 To examine this relationship another way, we conducted a linear regression analysis of
228 steroidogenic cell type area (independent variable) vs. cosyntropin-stimulated CORT
229 (dependent variable) at these same timepoints. This yielded a regression model of $Y =$
230 $0.016X - 3.9$ (R^2=0.43, p=0.0012; Fig. 5G). As visualized by an actual vs. predicted residual
231 plot, measured cosyntropin stimulated CORT levels were >50% lower at 1-2 weeks post-
232 withdrawal than predicted by the steroidogenic cell area at these same timepoints (5.0 vs. 10
233 mcg/dL at 8+1 and 5.0 vs. 11 mcg/dL at 8+2, Fig. 5H). Measured stimulated CORT secretion
234 roughly matched and then exceeded the predicted values 6 and 8-weeks post-withdrawal,
235 respectively (11 vs. 12 mcg/dL at 8+6 and 25 vs. 13 mcg/dL at 8+8). Overall, these analyses
236 demonstrate that CORT secretion is disproportionately low relative to the size of the recovering
237 non-histiocyte, adrenocortical cell compartment in the first two weeks after long-term DEX
238 treatment. As both basal and stimulated ACTH were elevated at these same time points (Fig. 2C
239 and E), this is consistent with adrenocortical atrophy with superimposed, secretory hypo-
240 responsiveness to ACTH.

241

242 *Maintenance of endogenous ACTH secretion but not intermittent cosyntropin administration*
243 *during the period of DEX exposures prevents GIAI*

244 After identifying the adrenal as the primary anatomical site of post-withdrawal HPA axis
245 dysfunction, we investigated whether GIAI could be prevented by providing trophic stimulation to
246 the gland during DEX exposure, a period when hypothalamic-pituitary function is otherwise
247 suppressed (Fig. 2A, B, C, and E, 8+0 timepoint). We first did this pharmacologically by
248 administering daily, intraperitoneal injections of cosyntropin, a synthetic ACTH analog (1-24) at
249 16:30, which coincides with the physiologic, circadian ACTH peak in rodents[33]. Mice were
250 concurrently treated with DEX via drinking water, as above (Model 2, Fig. 1). Following 8 weeks
251 of combined DEX+COS treatment, both agents were withdrawn, and adrenal recovery was

252 assessed with serial cosyntropin-stimulation testing at 1–2-week intervals until 8 weeks after
253 treatment cessation. At the time of treatment withdrawal (8+0), stimulated CORT secretion was
254 as low in DEX+COS-treated (2.0±1.0 mcg/dL) vs. DEX-treated animals (2.0±0.61 mcg/dL, 0.99).
255 Post-withdrawal, stimulated CORT secretion recovered more slowly in mice treated with
256 DEX+COS vs. DEX alone, with doubling times of 5.2 weeks ($Y = 3.8 * e^{0.13X}$; r^2=0.4) vs. 2.5
257 weeks ($2.6 * e^{0.28X}$, r_2=0.9), respectively, in exponential growth models (p=0.0009 for comparison
258 of fits by extra sum-of-squares F test; Fig. 6A).

259 Next, we tested whether maintenance of endogenous ACTH secretion, unlike intermittent,
260 pharmacologic administration, prevented DEX-induced adrenal suppression (Model 3, Fig. 1).
261 To do this, we bred $Sim1^{Cre}$:$GR^{fl/fl}$ mice (HGRKO), which have selective, hypothalamic deletion
262 of the glucocorticoid receptor (GR), leading to high basal Crh, ACTH, and CORT levels, the
263 latter of which are not diminished by an overnight dexamethasone-suppression test[34]. By
264 immunofluorescent analysis, GR was absent in 77% of PVH cells in HGRKO mice vs. 6% in
265 their Cre-negative (HGRWT) or functionally WT littermates (p<0.001, Fig. 6B and D). As
266 expected, PVH *Crh* mRNA expression was significantly higher in DEX-treated (8+0) HGRKO
267 (244±2.2 arbitrary units [AU]) vs. HGRWT animals (49±12 AU, p<0.01, Fig. 6C and E). Basal,
268 pre-treatment ACTH levels were higher in HGRKO (470±76 pg/mL) vs. HGRWT mice (104±55
269 pg/mL, p<0.05). At the completion of 8 weeks DEX treatment, ACTH levels were undetectable in
270 HGRWT animals (0±0 pg/mL) but preserved in HGRKO mice (385±64 pg/mL, p<0.01, Fig. 6F).

271 In the presence of this ongoing ACTH stimulation, adrenal weights were significantly higher
272 at the completion of DEX treatment in HGRKO (2.3±0.2 mg) vs. HGRWT animals (1.1±0.06 mg,
273 p≤ 0.001, Fig. 6G). Prior to DEX treatment, basal and stimulated CORT levels, via both a
274 psychological stressor (20 minutes physical restraint) and cosyntropin-stimulation testing, were
275 higher in HGRKO compared to HGRWT animals (Fig. 6H). Importantly, basal and stimulated
276 CORT levels on long-term DEX were markedly suppressed in HGRWT mice but robust in

277 HGRKO animals (basal: 1.5±0.98 in HGRWT vs. 14±1.6 mcg/dL in HGRKO, $p<0.01$; restraint
278 1.9±1.6 vs. 33±4.5 mcg/dL, $p<0.01$; cosyntropin-stimulated 1.1±0.62 vs. 33±3.9 mcg/dL,
279 $p<0.001$).

280 Cosyntropin-stimulated CORT levels were then directly compared for all 8+0 animals in
281 models 1, 2, and 3 (Fig. 1) to assess the efficacy of these pharmacologic or genetic strategies
282 for preventing GIA (Fig. 6I). At the time of DEX±COS withdrawal, CORT secretion was
283 suppressed in all treatment groups (WT DEX 8+0: 2.0±0.6; WT DEX+COS 8+0: 2.0±1.0;
284 HGRWT DEX 8+0 1.1±0.62 mcg/dL, $p<0.01$ for all vs. DN) except HGRKO mice (33±3.9
285 mcg/dL), which was significantly higher than DN controls ($p <0.01$).Thus, long-term DEX does
286 not suppress the HPA axis of HGRKO mice but does so in WT mice, including those co-treated
287 with intermittent cosyntropin.

288

289 *Short-term DEX-induced adrenocortical apoptosis is attenuated in cosyntropin-treated mice and*
290 *absent in HGRKO mice, but only HGRKO mice have preserved adrenal mass and morphology*
291 *on long-term DEX*

292 We next assessed whether our pharmacologic or genetic strategies protected mice against
293 DEX-induced adrenocortical apoptosis and atrophy. TUNEL staining was performed on adrenals
294 from WT animals treated for 4 days with either vehicle (DN), DEX, or DEX+COS as well as from
295 HGRKO animals treated for 4 days with DEX (Fig. 7A, B). This short-term timepoint permitted
296 investigation of active, DEX-induced adrenocortical apoptosis prior to major zF tissue loss. As
297 expected, 4 days of DEX induced significant adrenocortical apoptosis (TUNEL positive
298 cells=11±0.7% vs. 0.63±0.19% for DN, $p<0.001$). There were significantly fewer TUNEL-positive
299 cells in glands treated with DEX+COS (5.7±1.7%) vs. DEX alone (11±0.7%, $p<0.05$), albeit with
300 a bimodal distribution in which apoptosis was reduced by >65% in n=4 animals but comparable

301 to DEX-treated glands in the remaining n=3. TUNEL cells were uniformly fewer in HGRKO
302 animals (1.7±0.90%) such that there was no significant difference between these glands vs. DN
303 controls (p=0.97).

304 Adrenal morphology after long-term DEX treatment in either the pharmacologic (Model 2,
305 Fig. 1) or genetic (Model 3, Fig. 1) paradigms was then examined using thick, floating section
306 immunofluorescence for TH with 488-streptavidin, (as in Fig. 5), in WT DEX+COS 8+1, HGRWT
307 8+0, and HGRKO 8+0 glands (Fig. 7C). Pan-cortical, GHOST, and steroidogenic cell type areas
308 were all measured by morphometric analysis and normalized to DN controls from Model 1 (DN
309 data from Fig. 5B-D). Pan-cortical area decreased in WT DEX+COS 8+1 (0.68±0.15) but not
310 HGRKO 8+0 adrenals (1.3±0.09, p=0.02; Fig. 7D). Autofluorescent or GHOST area increased
311 >20x in 8+1 (22±6.4) yet was negligible HGRKO glands (2.8±2.3; Fig. 7E). Steroidogenic cell
312 type area was 62% (0.62+0.17) vs. 99% (0.99±0.02) of DN controls in WT DEX+COS 8+1 vs.
313 HGRKO 8+0 glands, respectively (Fig. 7F). Of note, 8+1 glands were heterogenous in their
314 cortical size and distribution of GHOSTs, such that one animal had a normal steroidogenic cell
315 type area with small GHOSTs interspersed throughout the zF (Fig. S3). HGRKO glands, on the
316 other hand, were uniformly normal in size and lacked GHOSTs. Our genetic but not
317 pharmacologic strategy of delivering trophic stimulation to the adrenal thus consistently prevents
318 short-term, DEX-induced adrenocortical apoptosis and preserves glandular size and
319 morphology on long-term treatment.

320

321 **DISCUSSION**

322 In this study, we investigated the timing of hypothalamic, pituitary, and adrenal recovery in
323 mice after 8 weeks of treatment with DEX to probe the mechanisms of protracted GIAI after
324 discontinuation of exogenous glucocorticoid therapy. Post-withdrawal central suppression of

325 hypothalamic-pituitary function is generally thought to be the limiting factor in the recovery of
326 adrenal function, and that once this occurs, adrenal function rapidly normalizes in response to
327 hypothalamic-pituitary stimulation. We found that hypothalamic-pituitary dysfunction recovers
328 rapidly after cessation of long-term, exogenous glucocorticoid treatment, whereas adrenal
329 function remains subnormal for a much longer period of time despite hypothalamic-pituitary
330 stimulation. We also found that long-term DEX treatment induces marked adrenal atrophy with
331 accumulation of giant, CD68- and F4/80-positive histiocyte clusters (GHOSTs), which persist
332 beyond recovery of adrenal function. However, even after accounting for the likely inability of
333 GHOSTs to produce glucocorticoids, CORT secretion is disproportionately low relative to the
334 remaining adrenocortical cell mass for at least 2 weeks post-DEX withdrawal despite
335 supraphysiologic ACTH stimulation during this time.

336 After we established the adrenal as the primary site of post-withdrawal HPA axis
337 dysfunction, we then asked whether trophic stimulation of the gland during the period of DEX
338 exposure can prevent GIAI, using both genetic and pharmacologic approaches. Mice with
339 feedback-resistant, sustained ACTH secretion due to deletion of the glucocorticoid receptor
340 gene (Gr, *Nr3c1*) from hypothalamic neurons (HGRKO) maintained normal adrenal function and
341 morphology throughout the entire period of long-term DEX treatment, while WT animals co-
342 treated with DEX and cosyntropin (DEX+COS) for the same amount of time had even slower
343 CORT recovery than those treated with DEX alone. In our short-term studies, DEX-induced
344 adrenocortical apoptosis was attenuated in both groups of mice, although this rescue was more
345 robust in DEX-treated HGRKO than in DEX+COS animals.

346 Our finding of early hypothalamic-pituitary recovery aligns with previous rodent studies
347 showing normal plasma ACTH and/or corticotroph *Pomc* mRNA levels within 1 week of
348 discontinuing 5-30 days of methylprednisolone or dexamethasone in mice and rats[22-24]. Ours is
349 the first preclinical study to examine HPA axis recovery after long term glucocorticoid therapy,

350 which is typically defined as greater than four weeks of supraphysiologic exposure and is most
351 strongly associated with GIAI development in humans[13]. Our model successfully reproduced
352 prolonged, severe CORT deficiency but lacked the initial period of hypothalamic-pituitary
353 dysfunction reported in prior clinical studies[16]. Of note, we did not evaluate hypothalamic-
354 pituitary status in the first week after steroid withdrawal, as any suppression at this time could
355 have been due to DEX-mediated negative feedback rather than to GIAI, given the long half-life
356 of the drug. Nonetheless, the lack of clinically significant, prolonged hypothalamic-pituitary
357 dysfunction in our model warrants investigation of the differences between the rodent and
358 human HPA axes as well as re-evaluation of the methodologies used to test for post-withdrawal
359 central suppression.

360 The 1965 Graber and Liddle study included only 6 patients with hypercortisolism from
361 exogenous glucocorticoid treatment who were studied after completing an undefined steroid
362 taper. Most importantly, ACTH levels were unable to be directly measured and were instead
363 derived from the CORT responses of hypophysectomized rats injected with extracted patient
364 plasma versus three standard doses of ACTH or saline[16,35]. During long-term prednisone
365 treatment in humans, ACTH responses to CRH stimulation and insulin-induced hypoglycemia
366 are suppressed. However, all testing in Graber et al. was performed 24 hours (~1-2 biological
367 half-lives) after prednisone administration, thus limiting the ability of the authors to distinguish
368 between active, glucocorticoid feedback inhibition vs. post-withdrawal central suppression[13,36].
369 In favor of early hypothalamic-pituitary recovery after steroid-induced adrenal suppression in
370 humans, patients with congenital adrenal hyperplasia, who also require chronic, suppressive
371 glucocorticoid therapy, have elevated levels of both ACTH and ACTH-dependent steroid
372 precursors just 12 hours (~3-4 have-lives) following a hydrocortisone dose[37,38]. The
373 discrepancies and methodologic limitations of the existing clinical literature, combined with our
374 finding of early, post-withdrawal hypothalamic-pituitary recovery in mice, highlight a need to

375 revisit this question with modern ACTH assays and larger numbers of glucocorticoid-treated and
376 -withdrawn patients .

377 Re-evaluating the paradigm of post-withdrawal central suppression has important
378 implications for defining the mechanisms underlying GIAI and developing effective preventative
379 strategies. First, if both basal and stress-induced ACTH secretion are rapidly restored after
380 discontinuing long-term glucocorticoids in humans, the latency in adrenal recovery that follows
381 reflects a period of ACTH hypo-responsiveness. This would be most likely presumed secondary
382 to adrenocortical atrophy given the well-established role of ACTH in preventing zF apoptosis
383 and maintaining proper adrenal zonation[9,10]. While we indeed found that DEX-treatment led to
384 adrenocortical apoptosis followed by major zF atrophy, adrenal weights recovered quickly
385 compared to CORT secretion after DEX was withdrawn. This aligns with prior preclinical studies
386 in which rodents had normal adrenal weights but low plasma CORT and/or adrenal
387 steroidogenic pathway gene expression within a week of discontinuing short-term (5-7 days)
388 glucocorticoid treatment[22-24]. With our finding of large, CD68+ and F4/80+ histiocyte clusters in
389 DEX-exposed glands, adrenal weights may overestimate functional cortical regeneration after
390 long-term glucocorticoid treatment. However, even after excluding this myeloid compartment by
391 morphometric analysis, recovery of CORT secretion lagged behind that of adrenocortical mass
392 after DEX withdrawal. As a potential limitation, this finding is based on 2-dimensional (2D) areas
393 as a surrogate for 3-dimensional (3D) cell counts. We established that zF cellular density was
394 similar between DEX-withdrawn and untreated control mice at all examined post-withdrawal
395 time points, making adrenocortical area a reasonable proxy for cellularity. Moreover, 2D area
396 overestimates 3D volume early in recovery when the glandular radius is reduced[39]. Our
397 conclusion that CORT secretion is disproportionately low relative to the adrenocortical cell mass
398 in the first 2 weeks after DEX withdrawal is thus conservative and warrants future investigation
399 into the mechanisms of ACTH hypo-responsiveness in early, post-withdrawal GIAI.

400 We have found giant, multinuclear histiocyte clusters after long-term glucocorticoid
401 treatment. Using electron microscopy, Wyllie and Kerr observed apoptotic cell bodies within
402 histiocyte phagosomes in rat adrenals after two days of prednisolone treatment[10]. Large, CD68-
403 and F4/80-positive histiocytes resembling GHOSTs were reported in aging male Znrf3 knockout
404 mice, which exhibit cortical hyperplasia followed by senescence[40]. In our studies, numerous
405 mononuclear macrophages were observed throughout the zF by 1-week of DEX, which
406 coincided with massive adrenocortical apoptosis by TUNEL staining. With ongoing DEX
407 treatment, these cells appeared to aggregate into giant clusters at the corticomedullary junction.
408 GHOSTs resembled multinucleated giant cells by both H&E and CD68 staining, but IF with the
409 membrane-bound macrophage marker F4/80 revealed a morphologic pattern consistent with
410 fusion of multiple, smaller multinucleated histiocytes. Interestingly, multinucleation and fusion of
411 phagocytic cells has been described in adipose tissue, ovary, and bone when demand for
412 cellular clearance is high[41-43]. We hypothesize that the massive adrenocortical apoptosis that
413 accompanies corticosteroid treatment leads to recruitment and/or expansion of an adrenal
414 macrophage population, which subsequently undergo fusion and multinucleation, perhaps for
415 enhanced phagocytic capacity.

416 Notably, GHOSTs remained abundant in the early weeks after DEX treatment when the
417 hypothalamus and pituitary had recovered but adrenal secretory capacity remained
418 disproportionally low for cortical size, raising the possibility that these histiocytes may disrupt
419 steroidogenesis. Adrenal macrophages have been reported to restrict CORT production via
420 paracrine signaling after undergoing activation in response to acute and chronic stress[44].
421 Specifically, intra-adrenal cortisol upregulates triggering receptor on myeloid cells 2 (Trem2) in
422 adrenal macrophages in a GR-dependent manner[44]. This promotes TGFβ secretion and
423 ultimately downregulation of steroidogenic acute regulatory protein (stAR) in adrenocortical
424 cells, which is the rate limiting enzyme in CORT biosynthesis[44-46]. In our studies, rising ACTH

425 and thus intra-adrenal CORT after DEX withdrawal may activate an expanded adrenal
426 macrophage population, providing one potential mechanism of secretory hypo-responsiveness
427 to ACTH after long-term glucocorticoid treatment. Future studies will further characterize the
428 origin, phagocytic, and regulatory functions of this macrophage population and investigate their
429 contribution to prolonged GIAI.

430 Most importantly, refocusing the mechanisms of post-withdrawal GIAI to the adrenal, rather
431 than the hypothalamus or pituitary, suggests that we may be able to prevent prolonged
432 suppression by providing effective, trophic stimulation to the gland during the period of
433 glucocorticoid exposure. In this study, we were able to preserve adrenal function and
434 morphology with a genetic approach that provided constant, CRH-driven, endogenous ACTH
435 stimulation during long-term glucocorticoid therapy but not with daily, intraperitoneal cosyntropin
436 injections. There are several key differences between these two strategies that should be
437 considered in subsequent attempts to develop an effective, preventative pharmacologic
438 treatment. First, we selected cosyntropin (ACTH 1-24) rather than purified ACTH (1-39) for initial
439 long-term studies, as the truncated peptide is thought to be as biologically potent but less
440 antigenic than the full-length hormone[47,48]. While cosyntropin is widely used diagnostically to
441 acutely stimulate steroidogenesis, its trophic effects are largely unstudied[49].

442 ACTH is also likely constantly elevated in the HGRKO model vs. intermittent in our
443 pharmacologic model. Cosyntropin, like native ACTH, has a biologic half-life of only 10-30
444 minutes[47,48]. We had hoped to overcome this by by achieving an initial systemic ACTH activity
445 >200x greater than that of physiologic ACTH at the circadian peak or in response to stress, akin
446 to what is used for high-dose stimulation testing in humans[50,51]. Cosyntropin treatment statistically
447 significantly reduced short-term, DEX-induced adrenocortical apoptosis, suggesting that we
448 successfully delivered biologically active cosyntropin to the gland. Interestingly, we observed a
449 heterogenous effect of cosyntropin on both short-term DEX-induced adrenocortical apoptosis and

450 long-term zF size and morphology, whereas CORT secretion was uniformly suppressed after
451 long-term DEX+COS treatment. Future studies will investigate whether different properties of
452 ACTH exposure are necessary to maintain the steroidogenic machinery vs. promote zF growth
453 and/or survival. The failure of intermittent cosyntropin to prevent GIAI may be due to an
454 inadequate duration of ACTH exposure, as adrenal *Mc2r* mRNA is increased after 6-48h of ACTH
455 treatment but not within an hour of ACTH injection or 4 hours of physicial restraint[52-56].
456 Alternatively, ultradian pulsatility may be necessary for the full biologic activity of ACTH, as it is
457 for GnRH and PTH[57,58]. Consistent with our interventions using CRH vs. ACTH to prevent GIAI in
458 mice, in patients with Cushing syndrome due to either ectopic CRH or ACTH secretion, two with
459 ectopic CRH section had rapid recovery of HPA axis function after tumor removal without
460 perceptible HPA axis suppression, whereas a third patient with ectopic ACTH secretion had
461 prolonged adrenal suppression after tumor resection[59]. Future studies will explore the
462 mechanisms by which activation of the endogenous HPA axis but not intermittent cosyntropin
463 administration preventions GIAI as a prelude to the development of future, preventative
464 pharmacologic strategies.

465 As a potential limitiation, our sample sizes were relatively small to enable a broad, agnostic
466 survey of HPA axis recovery across multiple timepoints. Most analyses were still adequately
467 powered given relative homogeneity among experimental animals, particularly when hormonal
468 function was interrogated with provocative tasting rather than basal measurements, as is done in
469 clinical endocrine practice. Nonetheless, subsequent mechanistic and interventional studies will
470 include larger cohorts of animals now that key, biologically relevant timepoints have been
471 identified. Similarly, the present study included only male mice to minimize biological variability
472 across this broad, initially exploratory survey of HPA axis recovery. While there are no reported
473 sex differences in the risk, severity, or duration of GIAI in humans[12,19,60,61], female rodents have
474 have more responsive HPA axes to stress as well as more rapid adrenocortical turnover, the latter
475 of which uniquely involes a capsular stem cell pool[62-67]. Warde et al. further reported more robust

476 adrenal CD68+ myeloid cell accumulation following cellular senescence in male vs. female Znrf3
477 knockout mice, which raises the possibility that the presence and functional consequences of
478 adrenal macrophages could be sexually dimorphic in our model[40,68]. Future studies will thus
479 specificially focus on sex-differences in the mechanisms of post-withdrawal GIAI and time to axis
480 recovery.

481 In conclusion, we have developed a physiological, preclinical model of GIAI in which long-term
482 glucocorticoids induce prolonged, adrenocortical dysfuntion in excess of glandular atrophy
483 despite rapid restoration of hypothalamic-pituitary function. Trophic stimulation of the gland during
484 the period of glucocorticoid exposure by nonsuppressible activation of the HPA axis, but not by
485 intermittent cosyntropin administration, prevents DEX-induced adrenal suppression. Future
486 studies will examine the mechanisms underlying adrenal hyporesponsiveness to ACTH in the
487 initial weeks after steroid withdrawal as well as those by which these two modes of adrenal
488 stimulation differentially protect against GIAI. This work may collectively guide the development
489 of novel therapies that prevent GIAI, thus decreasing the morbidity of one of our most widely
490 prescribed drug classes without sacrificing therapeutic efficacy.

491

492 **MATERIALS AND METHODS**

493 *Sex as a biological variable*

494 Our study exclusively examined male mice for reasons discussed (see Discussion above) and
495 to minimize biologic variability and thus adequately power a broad survey of HPA axis recovery
496 across multiple timepoints. Is it unknown whether the findings are relevant for female mice.

497

498 *Animals*

499 All animals protocols were in accordance with the National Institutes of Health guidelines and
500 were approved by the Animal Care and Use Committee of Boston Children's Hospital (Protocol
501 00001983). Mice were housed on a 12-hour/12-hour light-dark cycle (lights on at 7 am) with ad

502 libitum access to rodent chow and water unless otherwise indicated. Mice used for studies were
503 all aged either 8 weeks at the time of DEX initiation (long-term studies) or 8-16 weeks (DEX-naïve
504 controls or short-term studies).

505 ***Wild-type (WT) mice:*** C57BL/6J mice (The Jackson Laboratory, Bar Harbor, ME) were
506 maintained by breeding within our population.

507 ***Sim1^{Cre}:GR$^{fl/fl}$ mice (HGRKO):*** Sim1^{Cre} mice (generous gift of Brad Lowell, Beth Israel Lahey
508 Medical Center, Boston, MA) were bred to floxed GR exon 3 mice (B6.Cg-*Nr3c1$^{tm1.1Jda}$*/J, Catalog
509 #021021, The Jackson Laboratory, Bar Harbor, ME), both maintained on an inbred C57BL/6J
510 backround[34,69]. Littermates that were Cre negative but had GR exon 3 floxed alleles were used
511 as controls. Animals were genotyped using tail DNA extracted with 0.05 M NaOH, heated at 95°C
512 for 30 min and then neutralized with Tris-HCl (pH 7.4). All genotyping protocols used a 2x Taq
513 RED Master Mix, 1.5 mM $MgCl_2$ (Apex, 5200300-1250) with 10 μM diluted primers (IDT). Primers
514 and PCR protocols for each genotype are detailed in Table SI.

515 ***Pharmacologic treatments:*** Mice were treated with either water-soluble dexamethasone
516 (Sigma-Aldrich 2915) at a concentration of 3.6 mcg/mL (~20 mcg/day assuming an average water
517 intake of 5.8 mL/day[70]) or no-drug control via drinking water for either 4 days (short-term) or 8
518 weeks (long-term studies). When specified, mice were co-treated with 10 mcg/kg cosyntropin,
519 (synthetic ACTH 1-24, Sandoz, NDC 0781-3440-95), dissolved at 10 mcg/mL in 0.9% saline.
520 Cosyntropin was administered once daily by intraperitoneal injection at 16:30 p.m. to align with
521 the murine, circadian ACTH peak, for either 4 days or 8 weeks, as above.

522 ***Hormonal assays:*** All testing was performed, as specified, on separate days so that no
523 mouse was bled more than once on a given day. Plasma for measurement of corticosterone and
524 ACTH was obtained by rapid retroorbital phlebotomy without anesthesia into EDTA-coated
525 capillary tubes with a total time from first handling the animal to completion of bleeding not
526 exceeding 30 seconds. Blood was collected on ice, and plasma was separated by centrifugation

527 at 1500 RPM at 4°C and stored at -80°C until assay. Plasma concentrations of corticosterone
528 (ALPCO, 55-CORMS-E01) and ACTH (21-ACTHU-E01) were measured by ELISA per
529 manufaturer instructions. For the ACTH assay, plasma was diluted 1:10 with ACTH 0 calibrator
530 (ALPCO; 11-C-270-10-G25). The lower limit of detection is 0.061 mcg/dL and 0.22 pg/mL for the
531 CORT and ACTH assays, respectively.

532 - *Basal measurements:* Animals underwent rapid retroorbital phlebotomy, as above, at
533 16:30 in a ventilated hood in the same room as which the animals were housed.
534 Plasma ACTH and corticosterone were measured by ELISA as above.
535 - *Cosyntropin-stimulation testing:* Cosyntropin stimulation testing was performed 2
536 hours after lights on in ad libitum fed mice. Mice were bled by retroorbital phlebotomy
537 60 min after intraperiteoneal inection of 10 mcg/kg cosyntropin (10 mcg/mL in 0.9%
538 saline). Plasma CORT was measured by ELISA, as above[33].
539 - *Insulin-induced hypoglyemia:* Mice were deprived of food at lights off. The next
540 morning, within 2 hours of lights on, mice were intraperitoneally injected with
541 recombinant regular human insulin (Eli Lilly) at a dose of 1 u/kg, which was estimated
542 from previously published data to produce sustained hypoglycemia and consistent
543 pituitary-adrenal activation at 30-60 min after injection[71,72]. Mice were bled via
544 retroorbital phlebotomy for plasma hormone analysis (both ACTH and CORT) 40
545 minutes after injection[73]. Tail vein blood glucose was measured with a point-of-care
546 glucometer (FreeStyle Lite, Abbott) 60 minutes after insulin injection to document a
547 blood glucose nadir of <60 mg/dL, which occurred in all experimental animals.
548 - *Physical restraint:* Animals were confined in ventilated 50-mL conical tubes for 20
549 minutes followed by rapid retroorbital phlebotomy for plasma corticosterone
550 measurement.

551 ***Necroscopy and tissue preparation:*** Animals were euthanized by rapid decapitation without
552 anesthesia followed by necroscopy for isolation of hypothalami and adrenals. Coronal slabs
553 flanking the hypothalamus were prepared with a surgical blade and then fixed in 10% formalin
554 overnight before transfer to 70% ethanol while awaiting paraffin embedding. Adrenals were
555 trimmed of surrounding fat tissue, rinsed in phosphate-buffered saline (PBS), and weighed
556 before overnight fixation in 10% neutral buffered formalin.

557 ***Single-molecule RNA in situ hybridization***

558 Three 5mM-thick coronal brain sections were mounted onto each slide, and every other
559 slide was stained with hematoxylin and visualized with brightfield microscopy (Nikon E800). The
560 paraventricular nucleus was identified histologically based on its characteristic "butterfly-
561 shaped" appearance in coronal sections, which was used to anchor selection of 2 unstained
562 slides immediately rostral and caudal to this structure for analysis. Single-molecule RNA in situ
563 hybridization was performed using a catalog Mus musculus *Crh* probe (ACD #316091) and 2.5
564 HD RED detection kit (ACD #316091) following manufacturer's protocol. Slides were counter
565 stained with 50% Gill's Hematoxylin II and mounted with EcoMount. Positive control *Ppib (*ACD
566 #313911) and negative control *dapB (*ACD #310043) were used in every experiment to ensure
567 sample quality. Brightfield images at 40x magnification were generated with an Olympus VS120
568 Virtual Slide Scanner and then analyzed with semi-quantitative, densitometry using the Weka
569 Segmentation plugin for Fiji ImageJ per ACDBio instructions[74]. Analysis was restricted to free-
570 handed sections encompassing the characteristic "butterfly" morphology of PVH cell bodies, and
571 CRH expression, reported as arbitrary units (AU) was quantified by diving the area of the *Crh*
572 densitometric signal (μm^2) by the total area of this region (mm^2)

573

574 ***Total mRNA and protein staining***

575 For quantifying total mRNA *in situ*, FFPE sections were deparaffinized and antigen-retrieved
576 in buffer TE (pH=9). We then adapted the protocol in Farny *et al.* and Hurt *et al.* to label polyA-
577 capped RNAs on FFPE sections using Cy5-conjugated polyDT (26-4430-02, GeneLink)[26,27].
578 Total protein *in situ* was measured using the N-Hydroxysuccinimide (NHS) ester method; NHS
579 esters react with primary amines and well-approximate total protein mass[28,29]. Briefly, FFPE
580 sections were deparaffinized and antigen-retrieved in buffer TE (pH=9). Slides were stained with
581 NHS-Alexa 568 dye conjugates (Thermo Scientific A20003) in PBS for 30 minutes and then
582 washed 5X in PBS.

583

584 ***Paraffin section immunofluorescence***

585 After fixation, adrenals were oriented with their broadest surface parallel to the cutting plane
586 in 4% low-melting-temperature SeaPlaque agarose (Lonza, #50101). Agarose blocks were then
587 dehydrated in ethanol, xylene, and embedded in paraffin blocks. Paraffin sections were cut at 5
588 µm thickness. Sections were rinsed in xylene, an ethanol gradient, and then PBS. Antigen retrieval
589 was performed in either 10 mM Sodium Citrate pH 6.0 or Tris-EDTA pH 9.0 (Table SII). Sections
590 were blocked in 5% Normal Donkey Serum (NDS), 0.1% Tween-20 in PBS for 2h at RT. Slides
591 were then incubated in primary anitbodies diluted as below (Table SII) in 5% NDS at 4°C
592 overnight. Slides were washed three times for 5 min in 0.1% Tween-20 in PBS. Sections were
593 incubated for 2h at RT in secondary antibodies diluted 1:200 in PBS. For cortical counterstaining
594 in the CD68 experiment, Streptavidin, Alexa Fluor 488 Conjugate (Invitrogen, #S112233) was
595 added to the secondary antibody solution at a final concentration of 1:500. After three 5-min
596 washes with 0.1% Tween-20 in PBS, sections were incubated in TrueBlack Lipofuscin
597 Autofluorescence Quencher (Biotium, #23007) in 70% EtOH at RT for 3 minutes. Slides were
598 rinsed thee times in PBS and then mounted with Prolong Gold Antifade Mountant with DAPI
599 (Invitrogen, #P36931). For CD68 IF, Images were acquired with a Nikon Ti2 microscope with a

Yokogawa CSUW1 confocal unit, a Nikon Plan Apo Lambda 20x objective lens and a Zyla 4.2 PLUS sCMOS camera (ANDOR). All images were taken with identical laser strength, gain and exposure settings for the 488nM and 647nM channels. For all other experiments, fluorescent images were obtained with an Olympus VS120 Virtual Slide Microscope using a 20x objective. Brightness and contrast were adjusted for all images in ImageJ.

Floating section immunofluorescence.

After fixation, adrenals were oriented with their broadest surface parallel to the cutting plane in 4% low-melting-temperature SeaPlaque agarose (Lonza, #50101) and sectioned at a thickness of 100 µm with a vibratome. Individual slices were separated by free floating in PBS. Sections were wet-mounted in PBS on Superfrost Plus slides (Fisher Scientific, 12-550-15) and imaged with a 4x objective on a Nikon E800 brightfield microscope. The area of each section was measured in ImageJ, and the largest section was selected for subsequent immunostaining. Slices were washed three times with 0.1% Tween-20 in PBS and blocked in 5% normal donkey serum, 1% bovine serum albumin, and 0.1% Tween-20 in PBS for 1h at RT with gentle rocking. Slices were incubated with Sheep anti-tyrosine hydroxylase (1:500; Sigma Aldrich, #AB1542) diluted in blocking solution at 4°C overnight. After three 20 min washes with 0.1% Tween-20 in PBS, slices were incubated with Alexa Fluor 647-conjugated donkey anti-sheep IgG (1:100, Invitrogen, #A-21448) and Streptavidin, Alexa Fluor 488 Conjugate (1:500, Invitrogen, #S112233) diluted in 0.1% Tween-20 in PBS for 2h at RT. For nuclear staining, DAPI (4’6-diamino-2-phenylindole) was added to secondary antibody mix for the last 5 min at a final concentration of 1:1000. Slices were washed with 0.1% Tween-20 in PBS for 20 min three times and then directly mounted on Superfrost Plus Slides with Prolong Gold Antifade Mountant (thermo Fisher Scientific, #P36930). Images were acquired with a Nikon Ti2 microscope with a Yokogawa CSUW1 confocal unit, a Nikon Plan Apo Lambda 20x objective lens and a Zyla 4.2

PLUS sCMOS camera (ANDOR). All images were taken with identical laser strength, gain and exposure settings for the 405nm (used to capture autofluorescence), 488nm, and 647nm channels. Each image was acquired using the Large Image function in the NIS elements software. This function allowed us to take images in a 4x4 grid with 15% overlap, allowing the images to be stitched together. Brightness and contrast were adjusted for all images in ImageJ.

Image analysis

Fluorescent images were analyzed using QuPath (version 0.4.3), an open-source software for digital pathology.

Positive Cell Detection

QuPath's cell detection feature was employed to label cells as either Ki-67 or TUNEL positive based on co-localization of the 647 channel signal with the DAPI nuclear signal. Images were opened in fluorescence mode, and regions of interest (ROI) were mannually defined to include only the adrenal cortex based on morphologic characteristics. ROI were further restricted to the zF for Ki-67 analysis, as defined by DAB2-negative cortical cells. The "cell detection" feature was then run specifying DAPI as the detection channel and the 647 nm channel nuclear (Ki-67 analysis) or cellular (TUNEL analysis) mean as the score compartment. Nuclear size and intensity threshold parameters for both were adjusted and inspected visually to ensure accurate positive cell detection. Any cell exhibiting signal overlap between the DAPI and 647 nm channels above the specified thresholds was classified as either TUNEL or Ki-67 positive and reported as a percentage among total cells.

Morphometry

649 Morphometric analysis was performed on thick, floating section immunofluorescent
650 specimens to quantify the area of either the adrenal cortex (Strepatividin staining, 488 nm
651 channel), medulla (tyrosine hydroxylase immunostaining, 647 nm channel), or GHOSTs
652 (autofluorescence, 408 nm channel) based on signal intensity across multiple channels using the
653 "create thresholder" function in QuPath. Images were opened in fluorescence mode, and
654 brightness/contrast of individual channels were adjusted for optimal signal visualization. Regions
655 of interest were mannually defined to include the entire adrenal slice but not surrounding adipose
656 tissue. For each channel, QuPath's intensity thresholding was applied to ensure accurate
657 delineation of stained or autofluorescent areas, as confirmed by visual inspection. As DEX
658 treatment has been shown to attenuate streptavidin staining in the murine zF, we applied a lower
659 threshold in 8+0 adrenals to ensure detection of all residual adrenocortical tissue[31]. The area of
660 tissue with a signal above this threshold for each channel was classified as positive and reported
661 in square microns.
662
663 ***Statistics***
664 Two-tailed Student's t test was performed to compare significance among two groups.
665 Comparisons done beyond 2 groups were performed by ANOVA, and Bonferroni correction was
666 applied for post-hoc, pairwise multiple compraison testing. Nonlinear regression using an
667 exponential growth equation was used to model stimulated CORT recovery (dependent variable)
668 over time (independent variable), and doubling time was computed as ln(2)/K where K is the rate
669 constant. When two exponential growth models were compared, the extra-sum-of squares test
670 was employed to determine whether the exponential equations provided significantly different fits
671 to the data. The relationship between steroidogenic area (independent variable) vs. stimulated
672 CORT (dependent variable) was modeled by simple linear regression. Goodness of fit for all
673 regression analyses was reported as R^2 values. *P* values below 0.05 were considered statistically

674 significant. All statistical analyses were performed in Graphpad Prism v.10.3.1. Windows,
675 GraphPad Software, Boston, Massachusetts USA, www.graphpad.com
676
677 ***Study approval***
678 All animal experiments were approved by the Boston Children's Hospital Institutional Animal
679 Care and Use Committee (Protocol Number 00001983).
680
681 ***Data availability***
682 All raw data associated with findings presented in this manuscript are included in the
683 Supporting Data Values file and are available from the corresponding author upon reasonable
684 request.
685
686 **AUTHOR CONTRIBUTIONS**
687 LG and JM conceived the project and designed experiments. LG, BJ, and HF conducted
688 experiments, and LG analyzed the data. LG, MS, and BJ acquired microscopic images. LG wrote
689 the manuscript, which was edited by JM and MS. All authors approved the final version of the
690 submitted manuscript.
691
692 **ACKNOWLEDGEMENTS**
693 This study was supported by NIH 5T32DK007699-39 (LG), NIH F32DK131795-02 (LG), a
694 Pediatric Endocrine Society Research Fellowship Award (LG), a Pediatric Endocrine Society
695 Clinical Scholar Award (LG), a Boston Children's Hospital Office of Faculty Development/Basic &
696 Clinical Translational Research Executive Committees Faculty Career Development Fellowship
697 (LG), and the Thomas Morgan Rotch Harvard Medical School endowment (JAM). We thank Drs.
698 David Breault, Kleiton Borges, and Mesut Berber for their input on this project and assistance
699 processing adrenal tissue, identifying zonal markers, and performing thick, floating section

immunofluorescence. We also thank Suzanne White from the BIDMC Histology core for preparing and sectioning all FFPE specimens, including working closely with the author to isolate the PVH in mouse brains.

725 **FIGURES AND LEGENDS**

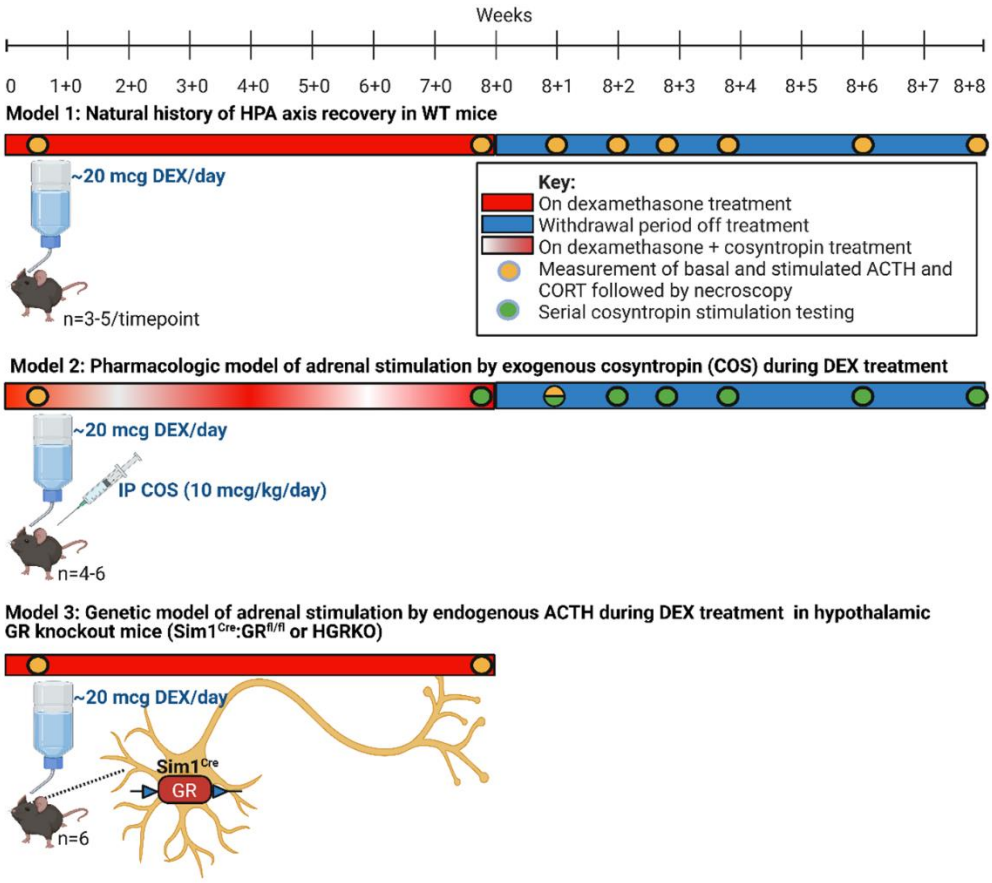

726

727 **Figure 1. Experimental design for dexamethasone (DEX) ± cosyntropin (COS) treatment**
728 **and withdrawal in wild-type (WT, Models 1 and 2) and HGRKO (*Sim1*^{Cre}:*GR*$^{fl/fl}$) (Model 3)**
729 **mice.** In model 1, the natural history of HPA axis recovery after long-term DEX was studied by
730 treating WT mice with 8 weeks of DEX (red bar) followed by serial assessments of axis function
731 and histology at 1-2 week intervals after DEX was withdrawn (blue bar). In cohort 1, basal,
732 unstimulated ACTH and CORT were serially measured at the above timepoints (yellow dots).
733 Subsequent cohorts of animals underwent provocative HPA axis assessment with cosyntropin
734 stimulation and insulin-induced hypoglycemia testing on successive days followed by
735 necroscopy at these same timepoints (yellow dots). Pharmacologic (model 2) and genetic
736 strategies (model 3) were then studied for their ability to prevent GIAI. In model 2, mice were co-
737 treated for 8 weeks with DEX and cosyntropin, an ACTH analog, followed by cosyntropin-
738 stimulation testing to assess adrenal function after both agents were withdrawn (green dots).
739 Necroscopy for histologic studies was performed in a separate cohort of mice 1-week post-
740 DEX+COS (8+1; split yellow and green dot). In model 3, HPA axis activity was assessed upon
741 completion of an 8-week DEX course (8+0) in mice with selective hypothalamic deletion of the
742 glucocorticoid receptor (HGRKO), which allows for ongoing, endogenous ACTH secretion on
743 GC therapy. ACTH and CORT were measured in the basal, unstimulated state followed by
744 provocative assessments (restraint stress and cosyntropin-stimulation testing on successive
745 days) and necroscopy[75].

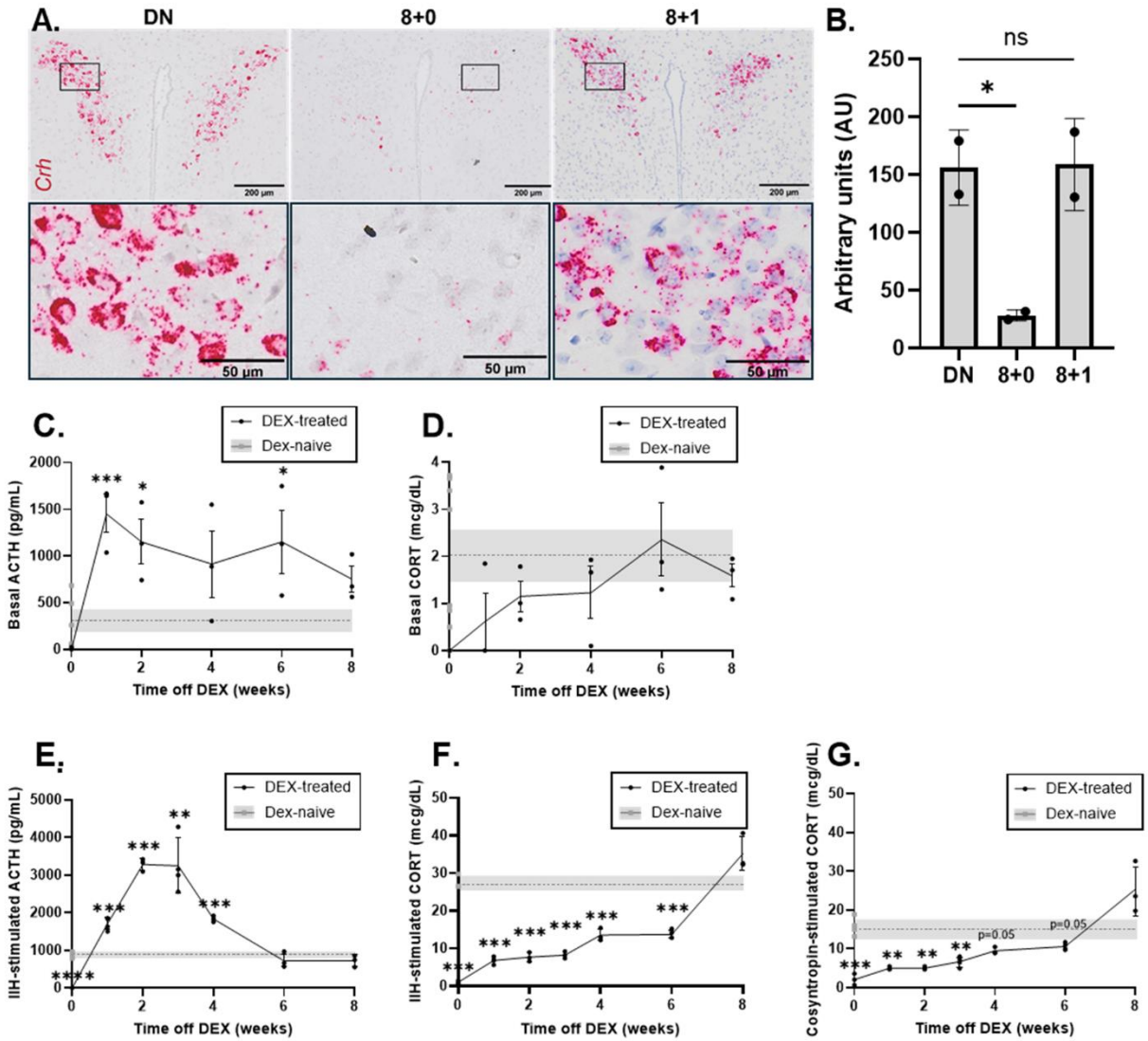

Figure 2. Stimulated CORT secretion requires 8 weeks to normalize after long-term DEX treatment despite early hypothalamic-pituitary recovery. A) *In situ* hybridization for basal *Crh* (red) in the paraventricular nucleus (PVH) of the hypothalamus in DEX-naïve (DN) animals and those treated with 8 weeks DEX both immediately prior to (8+0) and 1-week post-withdrawal (8+1; top row, scale bar=200 microns). Magnification of region within the black box is shown directly below (bottom row, scale bar=50 microns). B) Quantification of *Crh* mRNA expression from RNAScope images of the PVH from DN, 8+0, and 8+1 animals (n=2). $p<0.05$ by 1-way ANOVA. C) Recovery of plasma levels of basal (unstimulated), late afternoon ACTH and D) corticosterone (CORT) as well as E) insulin-induced hypoglycemia-stimulated ACTH, F) insulin-induced hypoglycemia-stimulated CORT, and G) cosyntropin-stimulated CORT 0-8 weeks after withdrawal of an 8-week DEX course. Data shown as individual mice with mean (connecting line) ± SEM (error bars). Grey bar (mean± SEM) indicates the reference range for adult, male, wildtype, untreated (DEX-naïve or DN) controls (n=4-8). * denotes $p<0.05$, ** $p<0.01$, *** $p<0.001$, and ****$p<0.0001$ vs. DN.

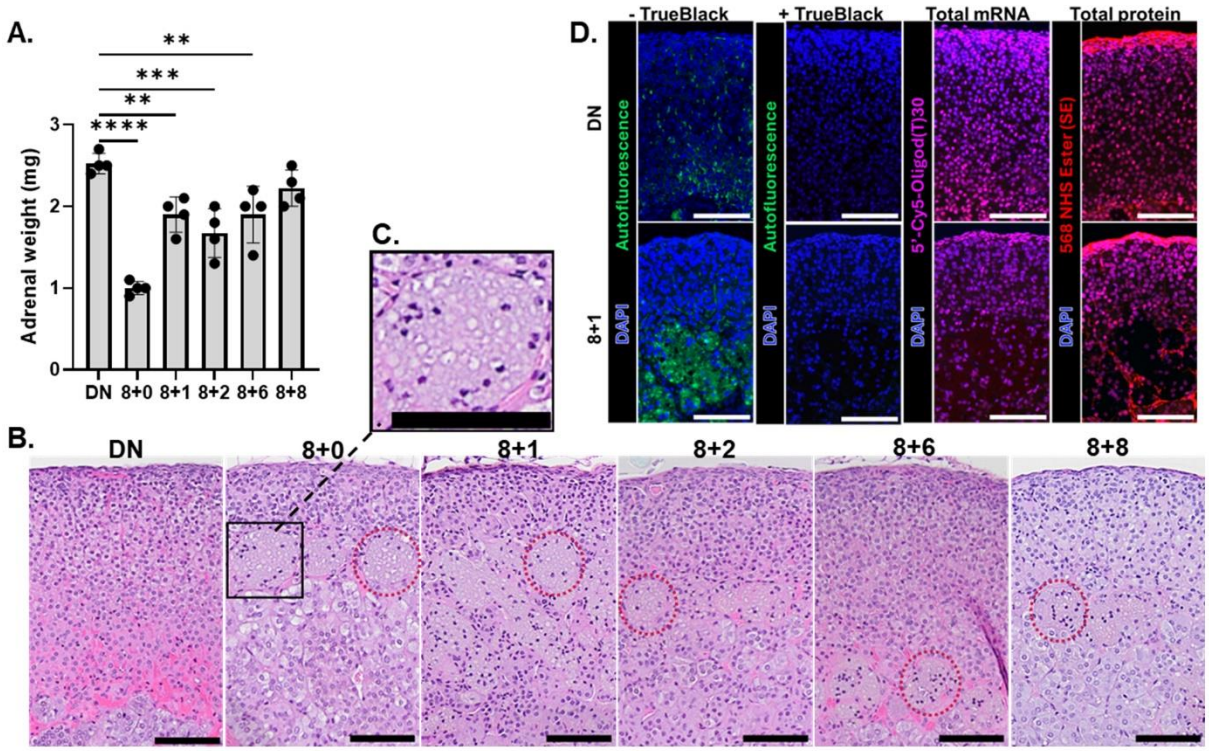

Figure 3. 8 weeks DEX induces adrenocortical atrophy with accumulation of poorly defined, vacuolated, cellular structures that persist through 8 weeks post-withdrawal. A) DEX-treated adrenals weigh significantly less than DN controls through 6 weeks post-withdrawal. P<0.0001 by one-way ANOVA; * indicates p<0.05, ** p<0.01, *** p<0.001, and ****p<0.0001 vs. DN. B) Hematoxylin and eosin staining reveals large, poorly defined, vacuolated structures with decreased nuclear density at the corticomedullary junction in DEX-exposed adrenals that persist through 8-weeks post-withdrawal. Representative structures are outlined with red, dashed circles and C) magnified (black box). D) These accumulations are present in DEX-exposed (8+1, bottom) but not DN adrenals (top) and are intensely autofluorescent (green). Autofluorescence is eliminated with the addition of TrueBlack, a lipofuscin autofluorescence quencher. Like surrounding adrenocortical cells, nuclei within these clusters contain mature mRNA (*in situ* hybridization for total polyA with 5'-Cy5-Oligo d(T)30; magenta) and protein (568 NHS Ester staining; red; both with TrueBlack). All scale bars=100 microns (B-D).

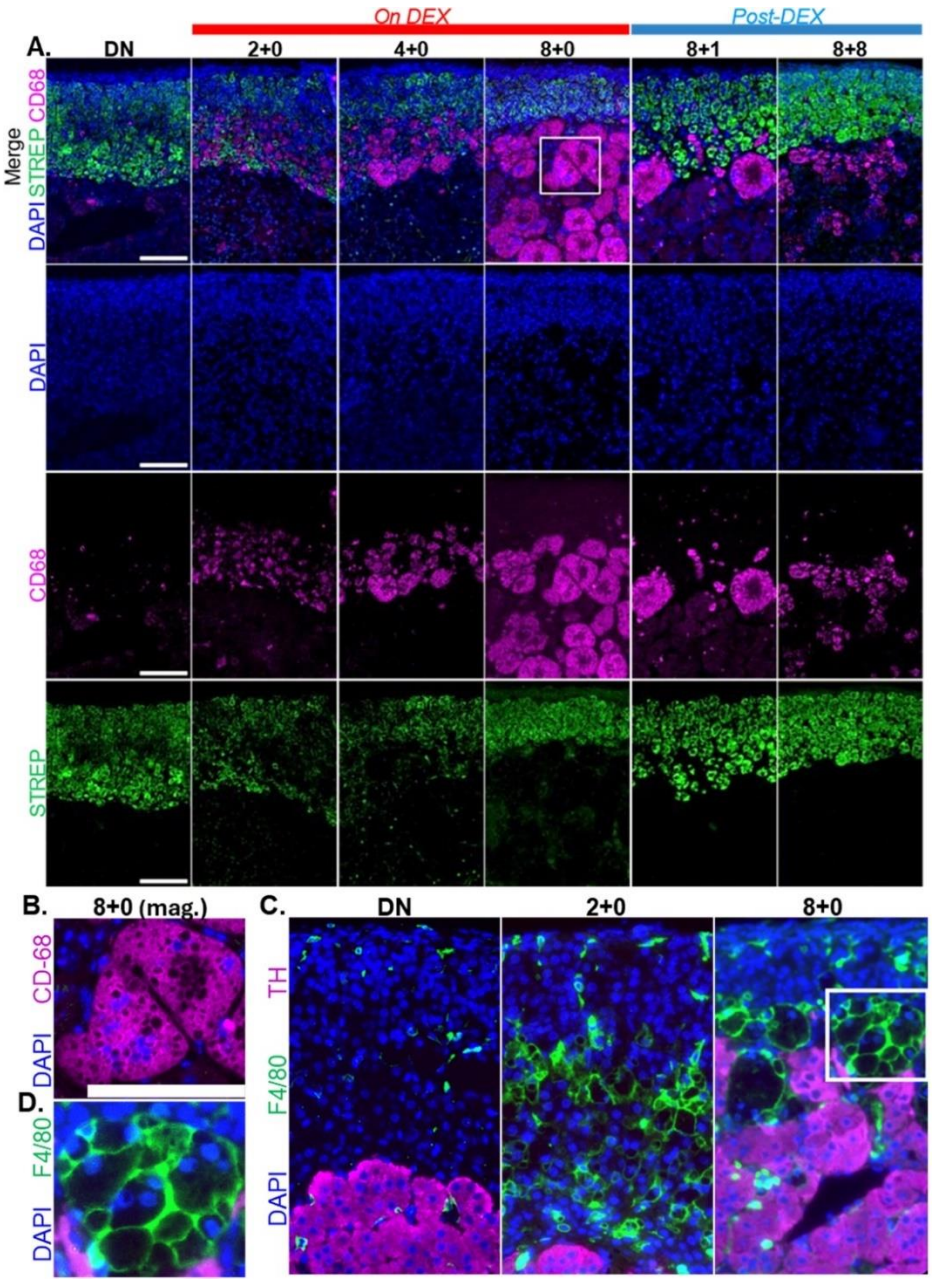

782

783 **Figure 4. Giant histiocyte clusters accumulate with prolonged glucocorticoid treatment**
784 **and persist through at least 8-weeks post-withdrawal.** A) Immunofluorescence for the
785 myeloid immune marker CD68 (magenta) with DAPI (blue) and 488-streptavidin (green)
786 counterstains, the latter of which labels all biotin-rich steroidogenic cells of the adrenal cortex.
787 Representative images shown for DN adrenals, those on DEX for 2-8 weeks (e.g. 2+0 to 8+0),
788 as well as one (8+1) and eight (8+8) weeks after an 8-week DEX course. B) Magnification of
789 representative CD68- positive cluster from an 8+0 gland. C) Immunofluorescence for the mouse
790 macrophage marker F4/80 (green) and medullary marker tyrosine hydroxylase (TH; magenta) in
791 DN and DEX-exposed adrenals (2+0 and 8+0). D) Magnification of F4/80-positive cluster from
792 an 8+0 gland. All staining performed with TrueBlack lipofuscin autofluorescence quencher (A-
793 D). All scale bars = 100 microns.

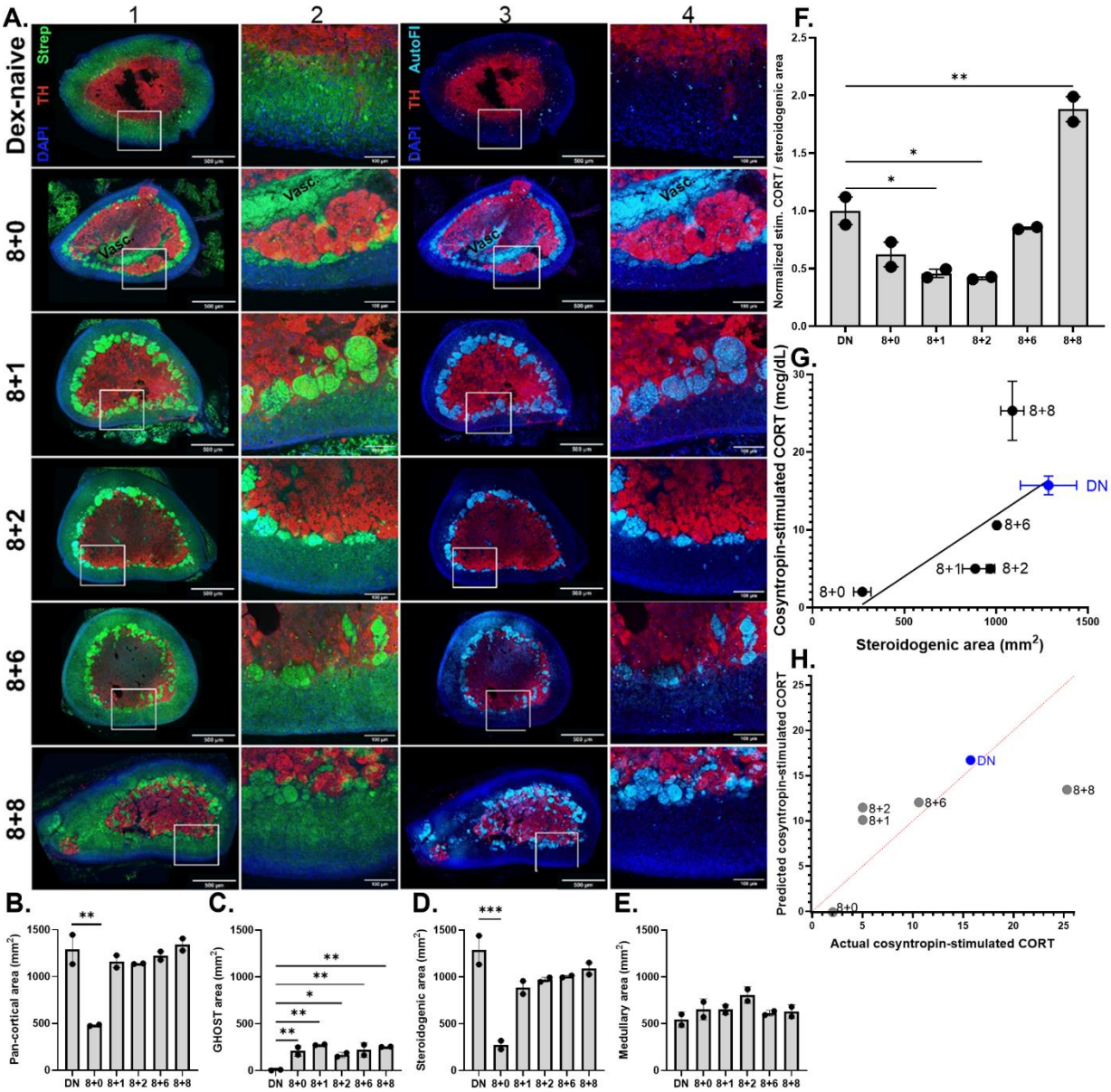

Figure 5. Stimulated CORT secretion is disproportionately low relative to adrenocortical cell mass in the first 1-2 weeks after withdrawal of long-term DEX. A) IF without TrueBlack for tyrosine hydroxylase (TH, red) DAPI (blue) and 488-streptavidin (green; columns 1 and 2) counterstains. Giant Histiocytes of Steroid Treatment (GHOSTs) were detected by autofluorescence (cyan; columns 3 and 4). Mice were either untreated (DN) or treated for 8 weeks DEX followed by withdrawal for 0-8 weeks (8+0, 8+1, 8+2, 8+6, and 8+8). Shown as 100 uM-thick, whole adrenal slices (columns 1 and 3, scale bar=500 microns) with magnification of the region in the white box (columns 2 and 4, scale bar=100 microns). Columns 1 and 2 imaged at wavelengths 405 nm, 488 nm, and 647 nm; columns 3 and 4 imaged at wavelengths 405 nm, 440 nm, and 647 nm. Morphometric analysis of B) pan-cortical area, which includes both streptavidin-positive and autofluorescent regions (p=0.0017cby one-way ANOVA), C) Autofluorescent GHOST area (p=0.0053 by one-way ANOVA), D) steroidogenic cell type area, calculated as pan-cortical area minus GHOSTs (p=0.0011 by one-way ANOVA), and E) medullary (TH- positive) area (p=0.15 by one-way ANOVA). F) Ratio of steroidogenic cell type area to cosyntropin-stimulated CORT secretion, normalized to DN controls. * p<0.05, ** p<0.01,

810 *** $p<0.001$ vs. DN (B-F). G). Linear regression analysis of steroidogenic cell type area
811 (independent variable) vs. cosyntropin-stimulated CORT secretion (dependent variable;
812 $R^2=0.43$, $p=0.0012$). H) residual plot from G) of actual vs. predicted cosyntropin-stimulated
813 CORT.

814

815

816

817

818

819

820

821

822

823

824

825

826

827

828

829

830

831

832

833

834

835

836

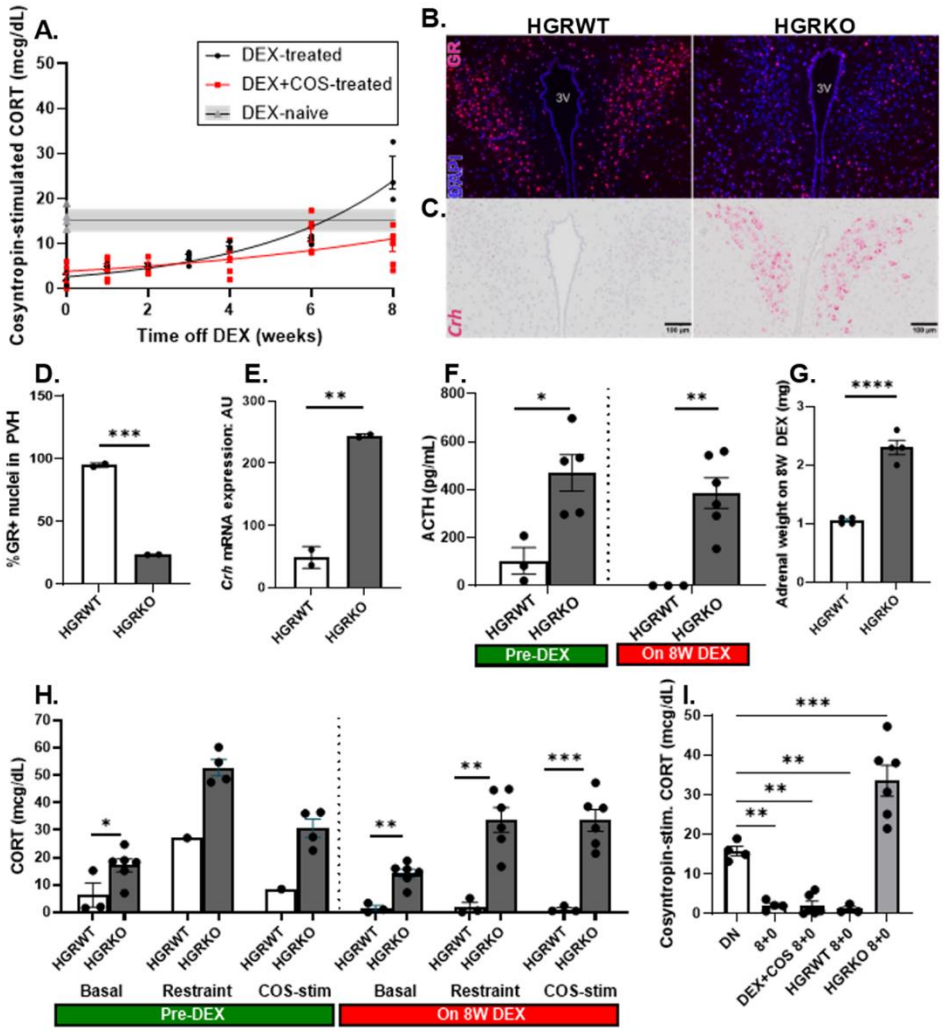

Figure 6. Endogenous ACTH secretion but not intermittent cosyntropin administration preserves adrenal mass and secretory function on long-term DEX treatment. A) Recovery of cosyntropin-stimulated CORT secretion in WT mice withdrawn from 8 weeks DEX+COS (red) vs. DEX-monotherapy (black). Data shown as individual mice with error bars centered on mean value ± SEM. Gray bar (mean ± SEM) indicates the reference range for adult, male, wildtype, DEX-naïve controls. Stimulated CORT recovery was modeled with exponential functions yielding doubling times of 5.2 weeks after DEX+COS ($Y = 3.8 * e^{0.13X}$ R^2=0.4, red curve) vs. 2.5 weeks after DEX ($Y = 2.6 * e^{0.28X}$; R^2=0.9, black curve). p= 0.0009 by extra sum-of-squares F test. B) IF for the glucocorticoid receptor (GR, red; DAPI, blue) in HGRWT (left panel) and HGRKO (right panel). C) *in situ* hybridization for *Crh* mRNA in the PVH of long-term DEX-treated Cre-negative control HGRWT (left panel) and Sim1^{Cre}:GR$^{fl/fl}$ HGRKO (right panel) animals. D) Quantification of the percentage of GR-positive nuclei and E) *Crh* mRNA expression in the PVH of HGRWT vs. HGRKO animals. F) Basal (unstressed circadian peak) ACTH levels in HGRWT vs. HGRKO animals prior to DEX (left of dashed line) and on 8 weeks of DEX (right of dashed line). p=0.19 for DEX status and p<0.0001 for genotype by two-way ANOVA. G) Adrenal weights on 8 weeks of DEX in HGRWT vs. HGRKO animals. H) CORT secretion in the

854 basal state, following 20 minutes of physical restraint (Restraint), and following cosyntropin
855 stimulation (COS-stim.) in HGRWT vs HGRKO animals, either prior to DEX treatment (left of
856 dashed line) vs. on 8 weeks of DEX (right of dashed line). * $p<0.05$, ** $p<0.01$, *** $p<0.001$ by t-
857 test (HGRWT vs. HGRKO (D-H). I) Comparison of cosyntropin-stimulated CORT levels after 8
858 weeks DEX treatment from experiments in Models 1, 2, and 3 vs. DN controls: DEX in WT
859 (8+0), DEX+COS in WT (DEX+COS 8+0), DEX in HGRWT (8+0), and DEX in HGRKO mice
860 (8+0). $p<0.0001$ by one-way ANOVA; ** $p<0.01$ and *** $p<0.001$ vs. DN.

861

862

863

864

865

866

867

868

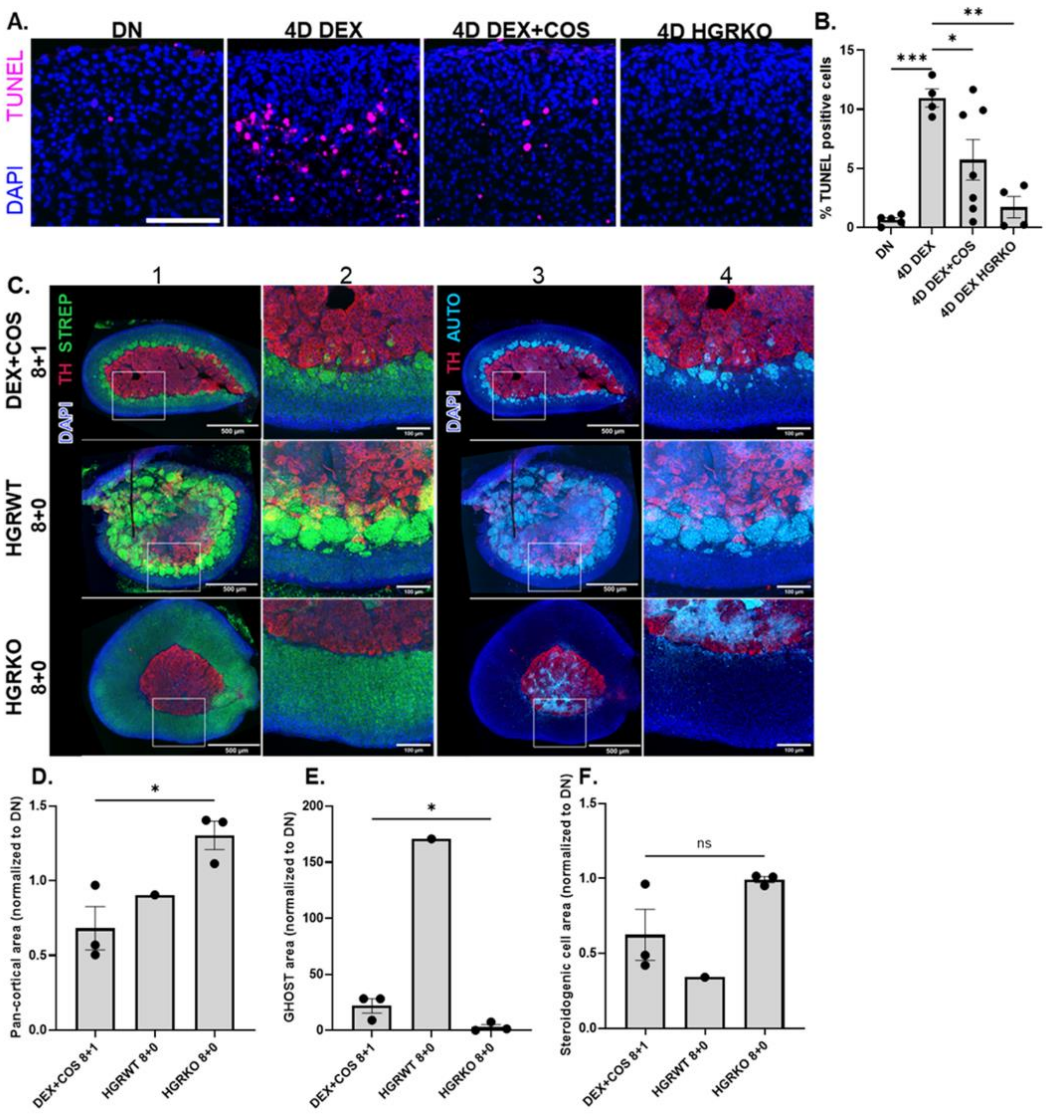

Figure 7. Intermittent cosyntropin attenuates short-term DEX-induced adrenocortical apoptosis, but only endogenous ACTH secretion maintains adrenal mass and morphology on long-term DEX treatment. A) Terminal deoxynucleotidyl transferase dUTP nick end labeling (TUNEL) in adrenals from WT mice treated for 4 days with vehicle (DN), DEX alone (4D DEX), or DEX with daily, intraperitoneal cosyntropin (4D DEX+COS), as well as DEX-treated HGRKO animals (4D HGRKO). B) quantitation of A) p=0.0004 by one-wav ANOVA**.** *p<0.05, ** p<0.01, *** p<0.001 for post-hoc multiple comparison testing. C) IF without TrueBlack for tyrosine hydroxylase (TH, red), with DAPI (blue), and 488-streptavidin (green) counterstains in columns 1 and 2. Giant Histiocytes of Steroid Treatment (GHOSTs) were detected by autofluorescence (cyan) in columns 3 and 4. Representative glands shown from WT animals 1-week withdrawn from 8 weeks combined DEX+COS (DEX+COS 8+1), see Fig. 1, Model 2; HGRWT on 8 weeks of DEX (8+0), and HGRKO on 8 weeks DEX (8+0), see Fig. 1, Model 3. 100 micron-thick, whole adrenal slices (columns 1 and 3, scale bar=500 microns) with magnification of the region in the white box (columns 2 and 4, scale bar=100 microns). Columns 1 and 2 are merged images at wavelengths 405 nm, 488 nm, and 647 nm; columns 3 and 4 are merged images at wavelengths 405 nm, 440 nm, and 647 nm. Morphometric analysis of D) pan-cortical area, which includes both streptavidin-positive and autofluorescent regions (p=0.0017

by one-way ANOVA), E) autofluorescent GHOST area (p=0.0053 by one-way ANOVA), F) steroidogenic cell type area, calculated as pan-cortical area minus GHOSTs (p=0.0011 by one-way ANOVA). Data in 7D are normalized to DN controls in Figure 5B; Data 7E are normalized to DN controls in Figure 5C; Data in 7F are normalized to DN controls in Figure 5D. * $p<0.05$ by t-test.

920 **References**

921 1. Fardet L, Petersen I, Nazareth I. Prevalence of long-term oral glucocorticoid prescriptions
922 in the UK over the past 20 years. *Rheumatology (Oxford).* 2011;50(11):1982-1990.
923 2. Overman RA, Yeh JY, Deal CL. Prevalence of oral glucocorticoid usage in the United
924 States: a general population perspective. *Arthritis Care Res (Hoboken).* 2013;65(2):294-
925 298.
926 3. Daley-Yates P, Brealey N, Thomas S, et al. Therapeutic index of inhaled corticosteroids in
927 asthma: A dose-response comparison on airway hyperresponsiveness and adrenal axis
928 suppression. *Br J Clin Pharmacol.* 2021;87(2):483-493.
929 4. Woods CP, Argese N, Chapman M, et al. Adrenal suppression in patients taking inhaled
930 glucocorticoids is highly prevalent and management can be guided by morning cortisol.
931 *European journal of endocrinology.* 2015;173(5):633-642.
932 5. Lam LH, Sugarman JL. Adrenal Suppression With Chronic Topical Corticosteroid Use in
933 Psoriasis Patients. *J Drugs Dermatol.* 2016;15(8):945-948.
934 6. Kachroo P, Stewart ID, Kelly RS, et al. Metabolomic profiling reveals extensive adrenal
935 suppression due to inhaled corticosteroid therapy in asthma. *Nature medicine.*
936 2022;28(4):814-822.
937 7. Keller-Wood ME, Dallman MF. Corticosteroid inhibition of ACTH secretion. *Endocrine*
938 *reviews.* 1984;5(1):1-24.
939 8. Wyllie AH, Kerr JF, Currie AR. Cellular events in the adrenal cortex following ACTH
940 deprivation. *The Journal of pathology.* 1972;106(1):Pix.
941 9. Pignatti E, Leng S, Carlone DL, Breault DT. Regulation of zonation and homeostasis in
942 the adrenal cortex. *Molecular and cellular endocrinology.* 2017;441:146-155.
943 10. Wyllie AH, Kerr JF, Macaskill IA, Currie AR. Adrenocortical cell deletion: the role of ACTH.
944 *The Journal of pathology.* 1973;111(2):85-94.

945 11. Younes AK, Younes NK. Recovery of steroid induced adrenal insufficiency. *Translational*
946 *pediatrics.* 2017;6(4):269-273.
947 12. Livanou T, Ferriman D, James VH. Recovery of hypothalamo-pituitary-adrenal function
948 after corticosteroid therapy. *Lancet (London, England).* 1967;2(7521):856-859.
949 13. Beuschlein F, Else T, Bancos I, et al. European Society of Endocrinology and Endocrine
950 Society Joint Clinical Guideline: Diagnosis and therapy of glucocorticoid-induced adrenal
951 insufficiency. *European journal of endocrinology.* 2024;190(5):G25-g51.
952 14. Ebrahimi F, Widmer A, Wagner U, et al. Association of adrenal insufficiency with patient-
953 oriented health-care outcomes in adult medical inpatients. *European journal of*
954 *endocrinology.* 2019;181(6):701-709.
955 15. Mebrahtu TF, Morgan AW, Keeley A, Baxter PD, Stewart PM, Pujades-Rodriguez M. Dose
956 dependency of iatrogenic glucocorticoid excess and adrenal insufficiency and mortality: a
957 cohort study in England. *The Journal of clinical endocrinology and metabolism.*
958 2019;104(9):3757-3767.
959 16. Graber AL, Ney RL, Nicholson WE, Island DP, Liddle GW. NATURAL HISTORY OF
960 PITUITARY-ADRENAL RECOVERY FOLLOWING LONG-TERM SUPPRESSION WITH
961 CORTICOSTEROIDS. *The Journal of clinical endocrinology and metabolism.* 1965;25:11-
962 16.
963 17. Avgerinos PC, Chrousos GP, Nieman LK, Oldfield EH, Loriaux DL, Cutler GB, Jr. The
964 corticotropin-releasing hormone test in the postoperative evaluation of patients with
965 cushing's syndrome. *The Journal of clinical endocrinology and metabolism.*
966 1987;65(5):906-913.
967 18. Avgerinos PC, Nieman LK, Oldfield EH, et al. The effect of pulsatile human corticotropin-
968 releasing hormone administration on the adrenal insufficiency that follows cure of
969 Cushing's disease. *The Journal of clinical endocrinology and metabolism.* 1989;68(5):912-
970 916.

971 19. Prete A, Paragliola RM, Bottiglieri F, et al. Factors predicting the duration of adrenal
972 insufficiency in patients successfully treated for Cushing disease and nonmalignant
973 primary adrenal Cushing syndrome. *Endocrine.* 2017;55(3):969-980.
974 20. Gomez MT, Magiakou MA, Mastorakos G, Chrousos GP. The pituitary corticotroph is not
975 the rate limiting step in the postoperative recovery of the hypothalamic-pituitary-adrenal
976 axis in patients with Cushing syndrome. *The Journal of clinical endocrinology and*
977 *metabolism.* 1993;77(1):173-177.
978 21. Denver RJ. Structural and functional evolution of vertebrate neuroendocrine stress
979 systems. *Annals of the New York Academy of Sciences.* 2009;1163:1-16.
980 22. Spiga F, Zhao Z, Lightman SL. Prolonged treatment with the synthetic glucocorticoid
981 methylprednisolone affects adrenal steroidogenic function and response to inflammatory
982 stress in the rat. *Brain Behav Immun.* 2020;87:703-714.
983 23. Calogero AE, Kamilaris TC, Johnson EO, Tartaglia ME, Chrousos G. Recovery of the rat
984 hypothalamic-pituitary-adrenal axis after discontinuation of prolonged treatment with the
985 synthetic glucocorticoid agonist dexamethasone. *Endocrinology.* 1990;127(4):1574-1579.
986 24. Duncan PJ, McClafferty H, Nolan O, et al. Corticotroph isolation from Pomc-eGFP mice
987 reveals sustained transcriptional dysregulation characterising a mouse model of
988 glucocorticoid-induced suppression of the hypothalamus-pituitary-adrenal axis. *Journal of*
989 *neuroendocrinology.* 2022;34(7):e13165.
990 25. Sakr N, Glazova O, Shevkova L, et al. Characterizing and Quenching Autofluorescence in
991 Fixed Mouse Adrenal Cortex Tissue. *Int J Mol Sci.* 2023;24(4).
992 26. Farny NG, Hurt JA, Silver PA. Definition of global and transcript-specific mRNA export
993 pathways in metazoans. *Genes Dev.* 2008;22(1):66-78.
994 27. Hurt JA, Obar RA, Zhai B, Farny NG, Gygi SP, Silver PA. A conserved CCCH-type zinc
995 finger protein regulates mRNA nuclear adenylation and export. *J Cell Biol.*
996 2009;185(2):265-277.

997 28. Liu X, Oh S, Kirschner MW. The uniformity and stability of cellular mass density in
998 mammalian cell culture. *Front Cell Dev Biol.* 2022;10:1017499.
999 29. Kafri R, Levy J, Ginzberg MB, Oh S, Lahav G, Kirschner MW. Dynamics extracted from
1000 fixed cells reveal feedback linking cell growth to cell cycle. *Nature.* 2013;494(7438):480-
1001 483.
1002 30. Almeida H, Ferreira J, Neves D. Macrophages of the adrenal cortex: a morphological study
1003 of the effects of aging and dexamethasone administration. *Annals of the New York*
1004 *Academy of Sciences.* 2004;1019:135-140.
1005 31. Paul A, Laufer E. Endogenous biotin as a marker of adrenocortical cells with steroidogenic
1006 potential. *Molecular and cellular endocrinology.* 2011;336(1-2):133-140.
1007 32. Romero DG, Yanes LL, de Rodriguez AF, et al. Disabled-2 is expressed in adrenal zona
1008 glomerulosa and is involved in aldosterone secretion. *Endocrinology.* 2007;148(6):2644-
1009 2652.
1010 33. Muglia LJ, Jacobson L, Weninger SC, et al. Impaired diurnal adrenal rhythmicity restored
1011 by constant infusion of corticotropin-releasing hormone in corticotropin-releasing
1012 hormone-deficient mice. *The Journal of clinical investigation.* 1997;99(12):2923-2929.
1013 34. Laryea G, Schütz G, Muglia LJ. Disrupting hypothalamic glucocorticoid receptors causes
1014 HPA axis hyperactivity and excess adiposity. *Molecular endocrinology (Baltimore, Md).*
1015 2013;27(10):1655-1665.
1016 35. Ney RL, Shimizu N, Nicholson WE, Island DP, Liddle GW. CORRELATION OF PLASMA
1017 ACTH CONCENTRATION WITH ADRENOCORTICAL RESPONSE IN NORMAL HUMAN
1018 SUBJECTS, SURGICAL PATIENTS, AND PATIENTS WITH CUSHING'S DISEASE. *The*
1019 *Journal of clinical investigation.* 1963;42(11):1669-1677.
1020 36. Schlaghecke R, Kornely E, Santen RT, Ridderskamp P. The effect of long-term
1021 glucocorticoid therapy on pituitary-adrenal responses to exogenous corticotropin-
1022 releasing hormone. *The New England journal of medicine.* 1992;326(4):226-230.

1023 37. Dauber A, Feldman HA, Majzoub JA. Nocturnal Dexamethasone versus Hydrocortisone
1024 for the Treatment of Children with Congenital Adrenal Hyperplasia. *Int J Pediatr*
1025 *Endocrinol.* 2010;2010.
1026 38. Mallappa A, Sinaii N, Kumar P, et al. A phase 2 study of Chronocort, a modified-release
1027 formulation of hydrocortisone, in the treatment of adults with classic congenital adrenal
1028 hyperplasia. *The Journal of clinical endocrinology and metabolism.* 2015;100(3):1137-
1029 1145.
1030 39. Stewart J, Clegg D, Watson S. *Calculus.* Cengage Learning, Incorporated; 2021.
1031 40. Warde KM, Smith LJ, Liu L, et al. Senescence-induced immune remodeling facilitates
1032 metastatic adrenal cancer in a sex-dimorphic manner. *Nat Aging.* 2023;3(7):846-865.
1033 41. Lazarov T, Juarez-Carreño S, Cox N, Geissmann F. Physiology and diseases of tissue-
1034 resident macrophages. *Nature.* 2023;618(7966):698-707.
1035 42. Foley KG, Pritchard MT, Duncan FE. Macrophage-derived multinucleated giant cells:
1036 hallmarks of the aging ovary. *Reproduction.* 2021;161(2):V5-v9.
1037 43. Braune J, Lindhorst A, Fröba J, et al. Multinucleated Giant Cells in Adipose Tissue Are
1038 Specialized in Adipocyte Degradation. *Diabetes.* 2021;70(2):538-548.
1039 44. Xu Y, Patterson MT, Dolfi B, et al. Adrenal gland macrophages regulate glucocorticoid
1040 production through Trem2 and TGF-β. *JCI Insight.* 2024;9(14).
1041 45. Miller WL. StAR search--what we know about how the steroidogenic acute regulatory
1042 protein mediates mitochondrial cholesterol import. *Molecular endocrinology (Baltimore,*
1043 *Md).* 2007;21(3):589-601.
1044 46. Miller WL, Bose HS. Early steps in steroidogenesis: intracellular cholesterol trafficking. *J*
1045 *Lipid Res.* 2011;52(12):2111-2135.
1046 47. Furman BL. Cosyntropin☆. In: *Reference Module in Biomedical Sciences.* Elsevier; 2017.

1047 48. Furman BL. Cosyntropin. In: Enna SJ, Bylund DB, eds. *xPharm: The Comprehensive*
1048 *Pharmacology Reference.* New York: Elsevier; 2007:1-3.
1049 49. Hamilton DD, Cotton BA. Cosyntropin as a diagnostic agent in the screening of patients
1050 for adrenocortical insufficiency. *Clin Pharmacol.* 2010;2:77-82.
1051 50. Dekkers OM, Timmermans JM, Smit JW, Romijn JA, Pereira AM. Comparison of the
1052 cortisol responses to testing with two doses of ACTH in patients with suspected adrenal
1053 insufficiency. *European journal of endocrinology.* 2011;164(1):83-87.
1054 51. Dickstein G, Spigel D, Arad E, Shechner C. One microgram is the lowest ACTH dose to
1055 cause a maximal cortisol response. There is no diurnal variation of cortisol response to
1056 submaximal ACTH stimulation. *European journal of endocrinology.* 1997;137(2):172-175.
1057 52. Mountjoy KG, Bird IM, Rainey WE, Cone RD. ACTH induces up-regulation of ACTH
1058 receptor mRNA in mouse and human adrenocortical cell lines. *Molecular and cellular*
1059 *endocrinology.* 1994;99(1):R17-20.
1060 53. Lebrethon MC, Jaillard C, Naville D, Bégeot M, Saez JM. Regulation of corticotropin and
1061 steroidogenic enzyme mRNAs in human fetal adrenal cells by corticotropin, angiotensin-
1062 II and transforming growth factor beta 1. *Molecular and cellular endocrinology.*
1063 1994;106(1-2):137-143.
1064 54. Lebrethon MC, Naville D, Begeot M, Saez JM. Regulation of corticotropin receptor number
1065 and messenger RNA in cultured human adrenocortical cells by corticotropin and
1066 angiotensin II. *The Journal of clinical investigation.* 1994;93(4):1828-1833.
1067 55. Rehman KS, Sirianni R, Parker CR, Jr., Rainey WE, Carr BR. The regulation of
1068 adrenocorticotrophic hormone receptor by corticotropin-releasing hormone in human fetal
1069 adrenal definitive/transitional zone cells. *Reprod Sci.* 2007;14(6):578-587.
1070 56. Liu Y, Smith LI, Huang V, et al. Transcriptional regulation of episodic glucocorticoid
1071 secretion. *Molecular and cellular endocrinology.* 2013;371(1-2):62-70.

1072 57. Stamatiades GA, Kaiser UB. Gonadotropin regulation by pulsatile GnRH: Signaling and
1073 gene expression. *Molecular and cellular endocrinology.* 2018;463:131-141.
1074 58. Chiavistelli S, Giustina A, Mazziotti G. Parathyroid hormone pulsatility: physiological and
1075 clinical aspects. *Bone Res.* 2015;3:14049.
1076 59. Lois KB, Santhakumar A, Vaikkakara S, et al. Phaeochromocytoma and ACTH-dependent
1077 cushing's syndrome: tumour crf secretion can mimic pituitary cushing's disease. *Clinical*
1078 *endocrinology.* 2016;84(2):177-184.
1079 60. Broersen LH, Pereira AM, Jørgensen JO, Dekkers OM. Adrenal Insufficiency in
1080 Corticosteroids Use: Systematic Review and Meta-Analysis. *The Journal of clinical*
1081 *endocrinology and metabolism.* 2015;100(6):2171-2180.
1082 61. Prete A, Bancos I. Glucocorticoid induced adrenal insufficiency. *BMJ.* 2021;374:n1380.
1083 62. Gao X, Yamazaki Y, Tezuka Y, et al. Gender differences in human adrenal cortex and its
1084 disorders. *Molecular and cellular endocrinology.* 2021;526:111177.
1085 63. Duncko R, Kiss A, Skultétyová I, Rusnák M, Jezová D. Corticotropin-releasing hormone
1086 mRNA levels in response to chronic mild stress rise in male but not in female rats while
1087 tyrosine hydroxylase mRNA levels decrease in both sexes. *Psychoneuroendocrinology.*
1088 2001;26(1):77-89.
1089 64. Viau V, Bingham B, Davis J, Lee P, Wong M. Gender and puberty interact on the stress-
1090 induced activation of parvocellular neurosecretory neurons and corticotropin-releasing
1091 hormone messenger ribonucleic acid expression in the rat. *Endocrinology.*
1092 2005;146(1):137-146.
1093 65. Goel N, Bale TL. Sex differences in the serotonergic influence on the hypothalamic-
1094 pituitary-adrenal stress axis. *Endocrinology.* 2010;151(4):1784-1794.
1095 66. Grabek A, Dolfi B, Klein B, Jian-Motamedi F, Chaboissier MC, Schedl A. The Adult Adrenal
1096 Cortex Undergoes Rapid Tissue Renewal in a Sex-Specific Manner. *Cell Stem Cell.*
1097 2019;25(2):290-296.e292.

1098 67. Hammer GD, Basham KJ. Stem cell function and plasticity in the normal physiology of the
1099 adrenal cortex. *Molecular and cellular endocrinology.* 2021;519:111043.
1100 68. Dolfi B, Gallerand A, Firulyova MM, et al. Unravelling the sex-specific diversity and
1101 functions of adrenal gland macrophages. *Cell reports.* 2022;39(11):110949.
1102 69. Tronche F, Kellendonk C, Kretz O, et al. Disruption of the glucocorticoid receptor gene in
1103 the nervous system results in reduced anxiety. *Nature genetics.* 1999;23(1):99-103.
1104 70. Bachmanov AA, Reed DR, Beauchamp GK, Tordoff MG. Food intake, water intake, and
1105 drinking spout side preference of 28 mouse strains. *Behav Genet.* 2002;32(6):435-443.
1106 71. Schreyer SA, Chua SC, Jr., LeBoeuf RC. Obesity and diabetes in TNF-alpha receptor-
1107 deficient mice. *The Journal of clinical investigation.* 1998;102(2):402-411.
1108 72. Daneva T, Spinedi E, Hadid R, Gaillard RC. Impaired hypothalamo-pituitary-adrenal axis
1109 function in Swiss nude athymic mice. *Neuroendocrinology.* 1995;62(1):79-86.
1110 73. Jacobson L, Muglia LJ, Weninger SC, Pacák K, Majzoub JA. CRH deficiency impairs but
1111 does not block pituitary-adrenal responses to diverse stressors. *Neuroendocrinology.*
1112 2000;71(2):79-87.
1113 74. Advanced Cell Diagnostics. (2019). TS-46-003 Technical Note: How to correctly interpret
1114 your RNAscope images. Rev B. Retrieved from https://acdbio.com/2019-mar-26-how-
1115 correctly-interpret-your-rnascope-images. In.
1116 75. Created in BioRender. Gaston, L. (2025) https://BioRender.com/v66r332

1117